CDF/ANAL/ELECTROWEAK/CDFR/2430

Measurement of $W\gamma$ and $Z\gamma$ Cross Sections in the Electron and Muon Channels with the 1992/1993 Data and Search for Anomalous $W\gamma$ and $Z\gamma$ Couplings

D. Benjamin[d], D. Errede[c], S. Errede[c], M. Lindgren[b], T. Muller[b], D. Neuberger[b], M. Timko[e], M. Vondracek[c], R.G. Wagner[a]

[a] *Argonne National Laboratory, Argonne, Illinois 60439*
[b] *University of California at Los Angeles, California 90024*
[c] *University of Illinois, Urbana, Illinois 61801*
[d] *Texas Tech University, Lubbock, Texas 79409*
[e] *Tufts University, Medford, Massachusetts 02155*

February 7, 1994

Abstract

We used the inclusive e, μ W and Z data samples obtained in the CDF '92-'93 collider run to study $W + \gamma$ and $Z + \gamma$ production. The analysis based on the full statistics of $21.8 \pm 2.2\ pb^{-1}$ ($20.6 \pm 2.1\ pb^{-1}$) of electron (muon) data. For central photons with $E_T^\gamma > 7.0\ GeV$ and $\Delta R_{\ell\gamma} > 0.7$, we observed 19 (7) electron (muon) $W\gamma$ candidates and 4 (4) electron (muon) $Z\gamma$ candidates. From these events, we derived values for $\sigma * BR(W\gamma)$ and $\sigma * BR(Z\gamma)$ for the electron, muon and combined e + μ samples and compared them to the Standard Model predictions. The P_T spectrum of the photons was used to obtain direct limits on anomalous $WW\gamma$ couplings which are: $-2.3 < \Delta\kappa < 2.2$ ($-2.3 < \tilde{\kappa} < 2.2$) and $-0.7 < \lambda < 0.7$ ($-0.7 < \tilde{\lambda} < 0.7$) at 95% CL. From these values, we extracted limits on higher-order EM moments of the W boson. Our results exclude a compositeness scale Λ_W in the W sector below 1.55 TeV at 95% CL for saturation of the unitarity bound. We have also obtained direct limits on anomalous $Z\gamma$ couplings.

1 Introduction

In the Standard Model of electroweak interactions the W, Z, and γ are considered to be fundamental gauge bosons. If the W and Z bosons were composite rather than fundamental, the rate of $W+\gamma$ and $Z+\gamma$ production would be higher than that predicted by the SM. In an earlier CDF note [1] we reported the observation of W and Z bosons produced in association with a photon, using the data from the 1988/1989 run, where CDF collected an integrated luminosity of $4.05 \pm 0.28 pb^{-1}$ of high P_T electron data and of $3.54 \pm .24 pb^{-1}$ of high P_T muon data. From our sample of 8(5) $W\gamma$ candidates and 2(2) $Z\gamma$ candidates in the electron (muon) decay channel we obtained a cross section times branching ratio measurement of this process, which was consistent with the Standard Model expectation, within a combined statistical and systematical uncertainty of about 60%. These findings are due to appear as a PRD, which has been distributed and to which we refer the reader for more detailed information on the physics of $WW\gamma$ and $ZZ\gamma$ /$Z\gamma\gamma$ processes.

This note reports the measurement of the $W + \gamma$ and $Z + \gamma$ production cross sections using the inclusive electron and muon W and Z data samples from the 1992/93 data run. A preliminary result was presented last year in CDF note 2143, which this note supercedes. Since that time much work has been done on backgrounds, systematic errors, and cross checking. Using the final samples, limits on anamalous couplings and moments have been obtained by using a new method which fits the P_T distribution of the photon.

The integrated luminosity was $21.8 \pm 2.2\ pb^{-1}$ for the electron data and $20.6 \pm 2.1\ pb^{-1}$ for the muon data. The samples of IVB events used were essentially the same as used in the "R analysis" (see below), except for the inclusion of events coming in on one additional level two trigger in the electron sample, in order to increase the sample statistics. The event sample was constructed by requiring an isolated, hard central photon with E_T greater than 7 GeV in each W or Z event. The data sample and analysis used to obtain it is described in section 2. The difficulty in the analysis lies primarily in the determination of the photon background, which can come from jets in the sample, (QCD background) or from real photons in background events in the sample. The QCD background was measured using the P16 data sample, as described in CDF note 2229, and briefly summarized in section 3. The other backgrounds, discussed in section 4, were measured using the same "fast" Monte Carlo program used to determine the predicted signal and measured cross sections, which is described in some detail in section 6.

Section 5 details the studies and measurements of the photon efficiencies, some of which have a P_T dependence. The acceptances and predicted number of signal events, calculated using a fast monte carlo simulation of the detector, are discussed in section 6. The systematic errors, determined by varying parameters in the generation of monte carlo events, are discussed in section 7. The cross section results for the four channels are presented in section 8. The data, background and predicted signals for standard and non-standard model couplings were used to extract limits on anomalous couplings by fitting to the E_T spectrum of the photons, as explained in section 9. The results are summarized in section 10.

2 Selection of Photon Candidates

The starting points for the analysis were the inclusive electron and muon data samples generated by Dave Saltzberg and Mark Krasberg. To obtain our W and Z samples we used the selection cuts which were used for the IVB cross section ratio analysis [2].

Electron W candidates were obtained from the common central electron sample by requiring $\not\!\!E_T > 20\ GeV$ in addition to the standard selection rules for the electron candidate [4]. The analysis also allowed events which passed one additional level two trigger(CEM_16_ISO_V3) and the standard level 3 trigger. This increased the fiducial electron trigger efficiency from the 89% value used in the R analysis, to 95%. This change was made after a study which looked for photons before looking for W candidates revealed that there were three events which pass all other W criteria except the one at level 2. Given the small statistics nature of the search, the trigger list was expanded to include these events. The W candidates were required not to be simultaneously consistent with being an electron Z candidate, as defined below. In addition, for events in the electron sample with an additional track with $P_T > 10$ GeV outside a jet the $\not\!\!E_T$ was recalculated using the track P_T, for tracks with $E/P < 1.0$, and events which failed the $\not\!\!E_T$ cut of 20 GeV after recalculation were rejected. This removed two events from the electron W sample which had high P_T tracks pointing to cracks in the calorimeter, which caused a significant miscalculation of the $\not\!\!E_T$. A total of 13920 events passed the electron W requirements.

Electron Z candidates were obtained from the common central electron sample by additionally requiring a second electromagnetic cluster of $E_T > 10.0\ GeV$ located in a good fiducial region of either the central, plug or forward calorimeters, where, amongst other technical requirements, the dielectron pair mass had to lie between $70 < M_{ee} < 110\ GeV/c^2$. A total of 1237 events passed the electron Z requirements.

The final muon W and Z samples used in this analysis were generated by Bill Badgett [3]. Muon W candidates were obtained from the common central muon sample by making an additional requirment of $\not\!\!E_T > 20\ GeV$. The W candidates were required not to be simultaneously consistent with being an muon Z candidate, as defined below. No CMX W candidates are used. A total of 6105 events passed the muon W requirements.

Muon Z candidates were obtained from the common central muon sample by additionally requiring a second minimum ionizing particle track of $P_T \geq 20\ GeV/c$ which - together with the muon candidate - had a beam-constrained dimuon pair mass $65 < M_{\mu\mu} < 115\ GeV/c^2$. A total of 507 events passed the muon Z requirements.

A common photon event selection was then additionally applied to each of these four inclusive data samples, to obtain the electron and muon $W\gamma$ and $Z\gamma$ sub-datasets. A photon candidate was defined by the following criteria.

- A 3 tower cluster of electromagnetic energy deposited in the central calorimeter of at least $E_T \geq 7\ GeV$, after position response and CEM energy scale correction.

- The location of the CEM cluster was required to be in a good fiducial

region of the central calorimeter, as defined by the position determined from CES shower centroid information and FIDELE fiducial cuts.

- The distance between the W/Z decay lepton(s) and the photon, $\Delta R_{\ell\gamma} = \sqrt{\Delta\eta^2 + \Delta\phi^2}$, must be greater than 0.7. This cut reduced largely the contribution of the radiative decay diagrams to the signal.
- The extra transverse energy deposited in a cone of $\Delta R = 0.4$ centered on the CEM cluster, but not including the EM cluster, divided by the E_T of the cluster($ET4/E_T$) must be less than 0.15.
- The extra summed transverse momentum($\sum PT4$) due to charged tracks within a cone of $\Delta R = 0.4$ centered on the CEM cluster must be less than 2.0 GeV. The tracks participating in the sum must have $|Z_{vtx} - Z_0| < 10\ cm$.
- No 3-D CTC tracks (originating from *any* vertex) pointing at the EM cluster (N3D=0).
- $Had/EM < 0.055 + 0.00045 * E$ where E was the total energy of the EM cluster in GeV.
- A three tower lateral shower-shape for the CEM cluster of $L_{shr} < 0.5$
- Using "11 channel clustering", the CES strip and wire chi-squares of a fit of the testbeam electron shower profiles to the leading cluster profile in each of these views, must each be less than 20.0
- Absence of 2^{nd} CES strip/wire clusters with $E_{CES\ 2^{nd}} > 1\ GeV$ (within the CEM cluster) was required to further suppress π^0 and multi-photon backgrounds.
- No second track with p$P_T > 10$ Gev outside a jet that forms a track-track mass with the W lepton track between 70 and 110 GeV(ee) or 40 and 140 GeV($\mu\mu$).

The numbers of events passing successive cuts are shown in table 1. With these selection rules we found 19 $W + \gamma$ and 4 $Z + \gamma$ candidates in the electron sample and 7 $W + \gamma$ and 4 $Z + \gamma$ in the muon sample. To illustrate the effect our photon cuts have on the data we show in Figures 1-3 the progression of cuts for the electron $W + \gamma$ sample. Figures 4-6 show the same cut progression for the muon $W + \gamma$ sample. The kinematic properties of individual events are listed in tables 2-5.

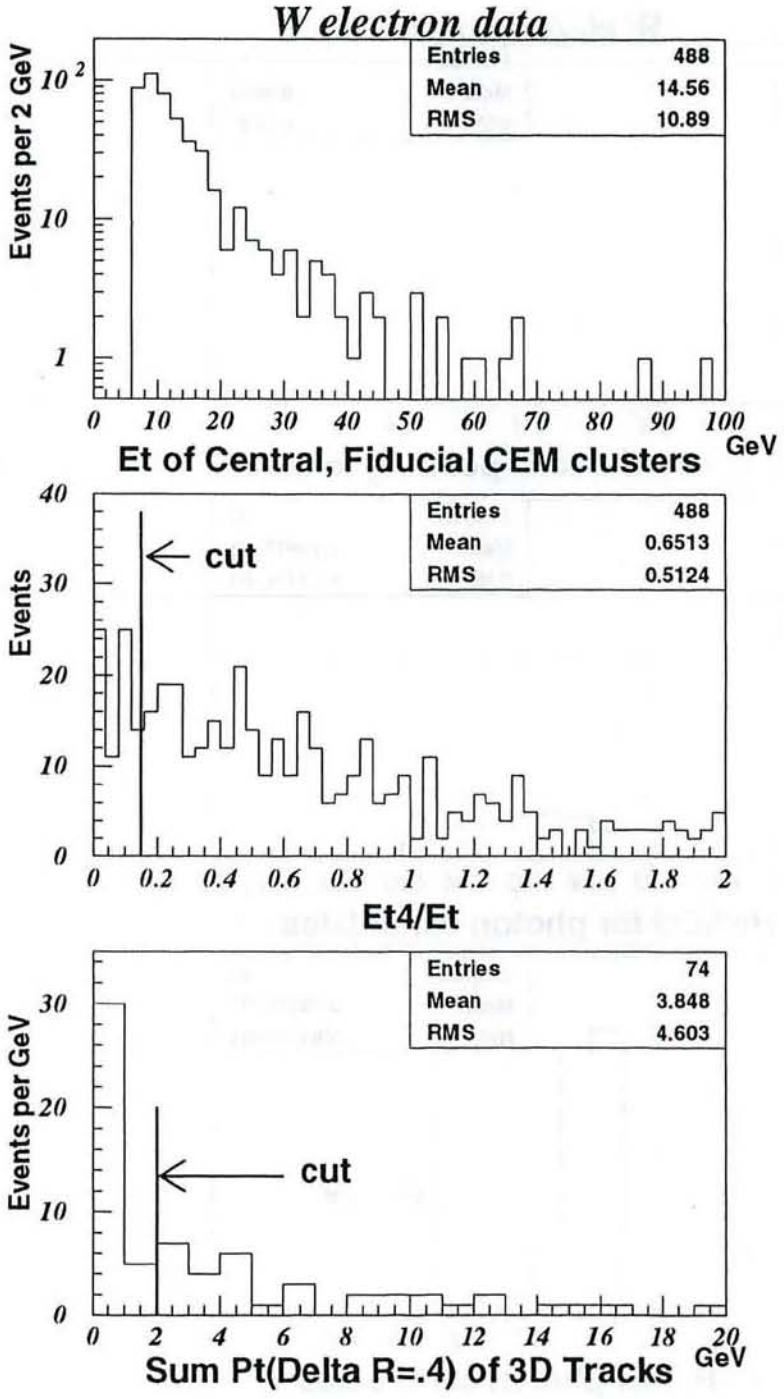

Figure 1: Et of Electromagnetic clusters, and effect of isolation cuts on those clusters in the electron W sample.

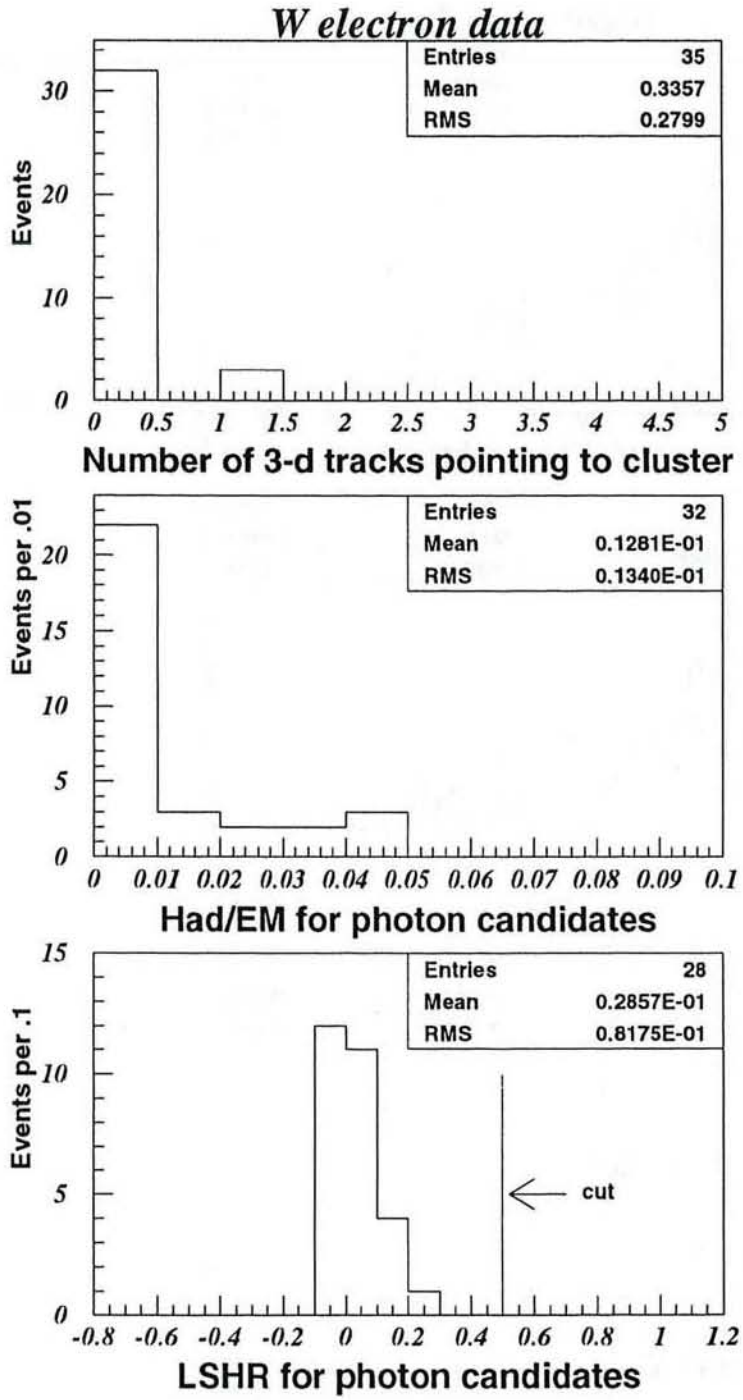

Figure 2: Additional photon cut variables, in the electron W sample.

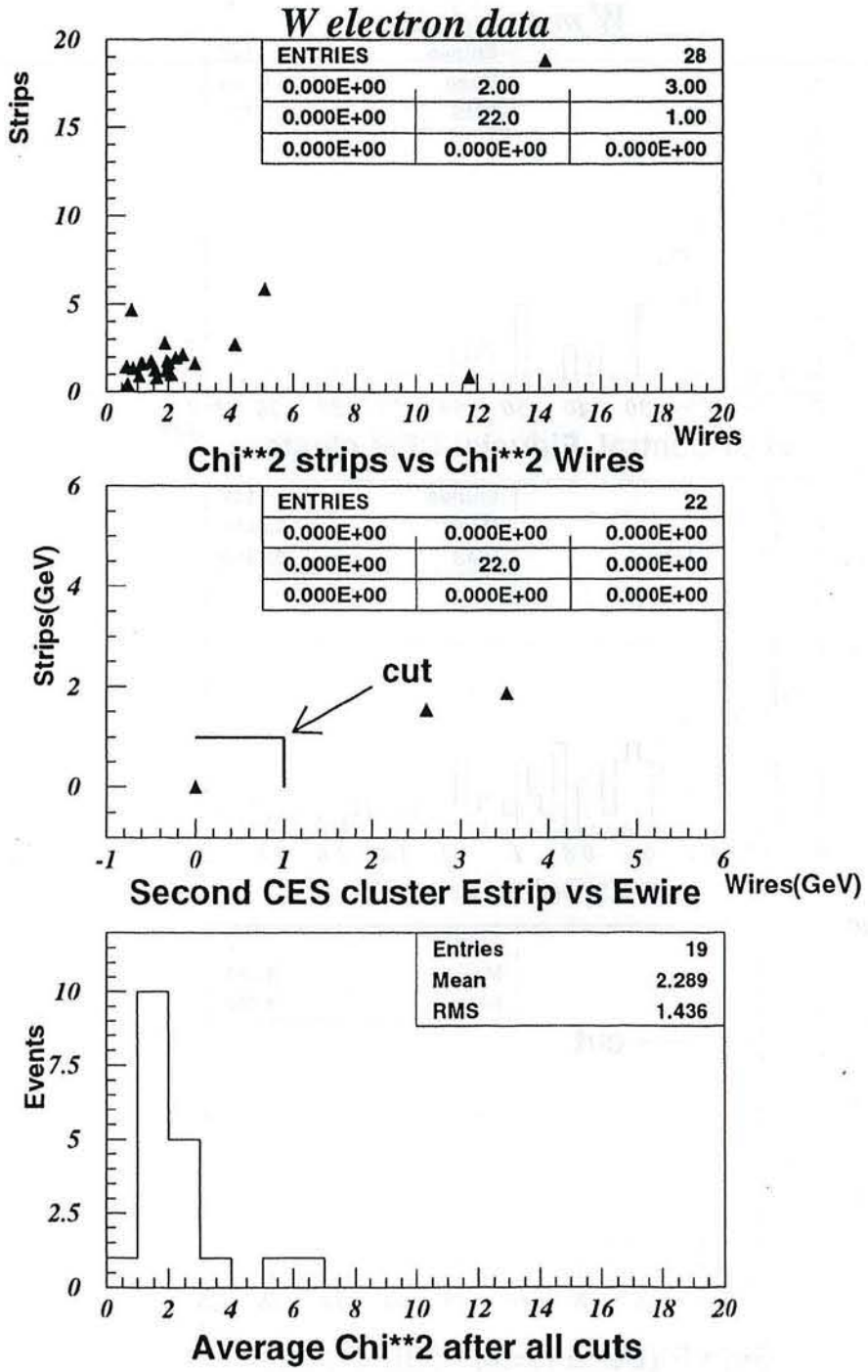

Figure 3: Photon Chi**2 and second cluster energies in the electron W sample.

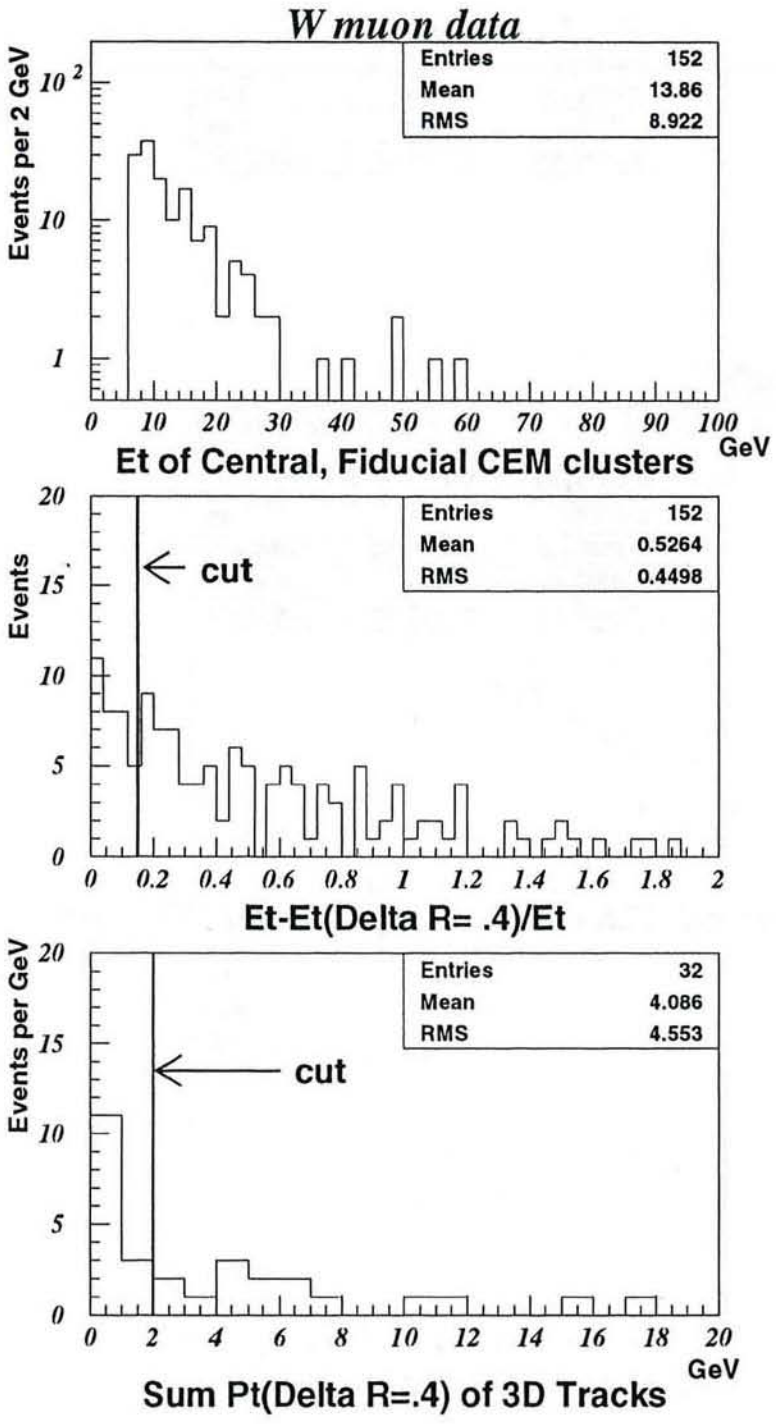

Figure 4: Et of Electromagnetic clusters, and effect of isolation cuts on those clusters in the muon W sample.

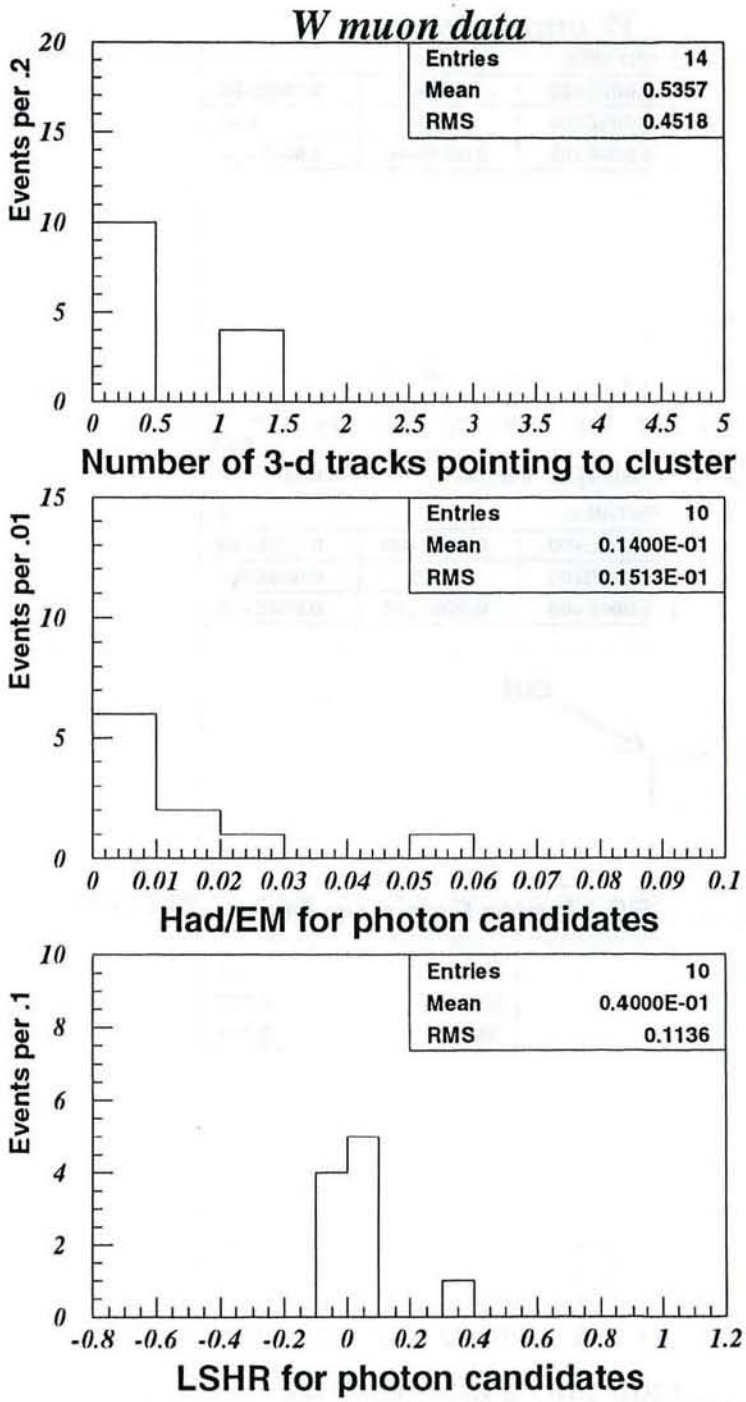

Figure 5: Additional photon cut variables, in the muon W sample.

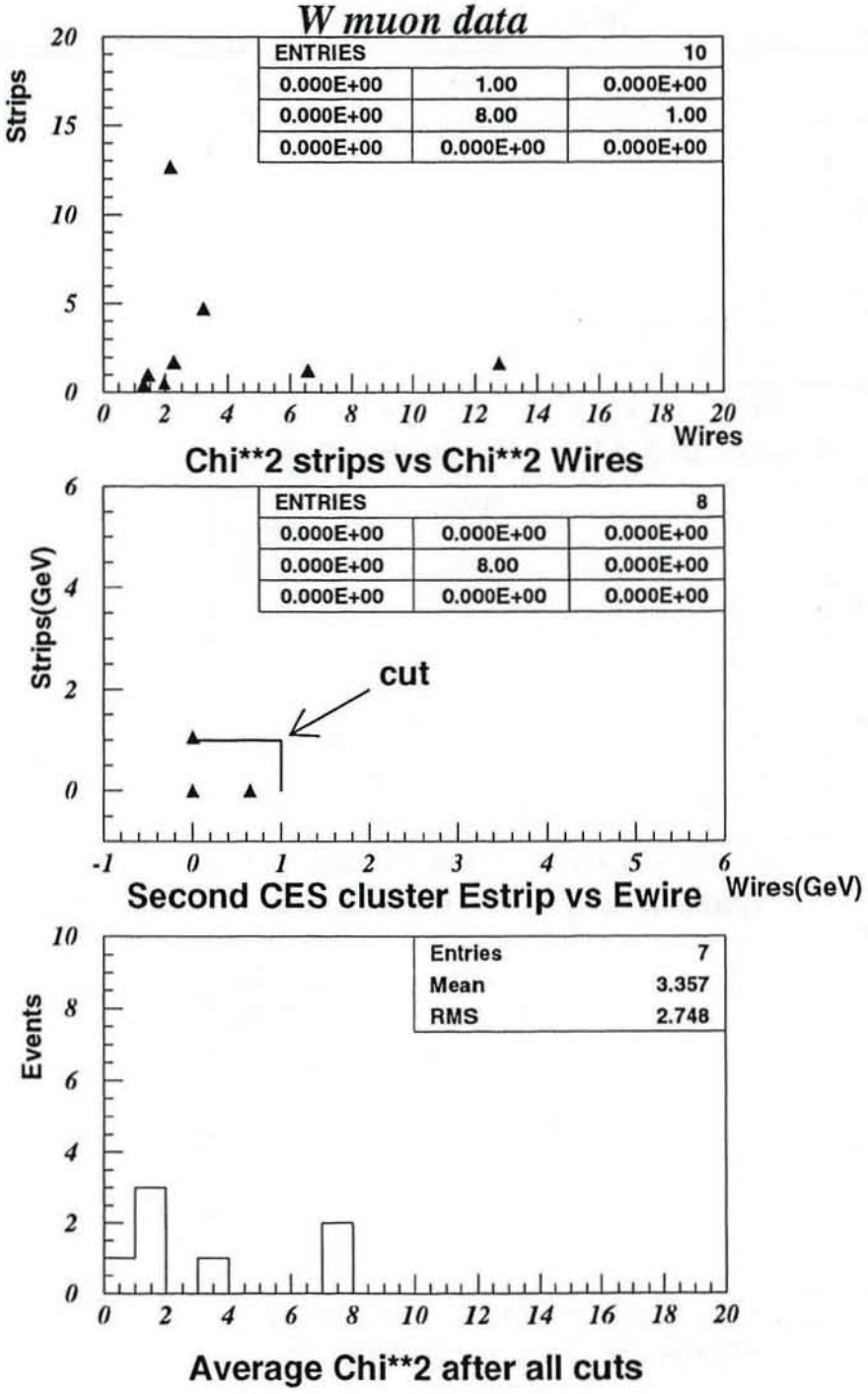

Figure 6: Photon Chi**2 and second cluster energies in the muon W sample.

	$W_e\gamma$	$W_\mu\gamma$	$Z_e\gamma$	$Z_\mu\gamma$	Pho-16$^{QCD}_{bkg}$
Inclusive W/Z or Photon-16 Samples	13920	6105	1237	507	6062
FidCEM, $E_T^\gamma > 7.0$ GeV, $\Delta R_{\ell\gamma} > 0.7$ Cuts	488	152	48	13	3067
$ET4/ET < .15$	74	32	14	4	704
$\Sigma PT4 < 2.0$ GeV	35	14	10	4	513
$N3D = 0$	32	10	9	4	–
Had/EM	32	10	9	4	507
$L_{shr} < 0.5$	28	10	7	4	407
$\chi^2_{strip} + \chi^2_{wire}$	22	8	6	4	287
no 2^{nd} $CES > 1$ GeV	20	7	4	4	216
no 2^{nd} Track ($W\gamma$ only)	19	7	–	–	–

Table 1: Summary of electron and muon $W\gamma$, $Z\gamma$ candidates and Photon-16 QCD background passing successive photon cuts. The entries in the first row of the first four columns are the number of inclusive W/Z events; the entries in the other rows of the first four columns are the number of W/Z events with fiducial CEM clusters surviving the successive photon cuts. In the last column, the first row is the number of central, fiducial, non-trigger ELES banks with no 3-D track pointing at it.

3 QCD Background

The main source of photon background in the $W\gamma/Z\gamma$ samples came from QCD jets misidentified as single isolated photons. This occurs when jets fragment into leading π^0's or η's with low numbers of other particles. We measured this background using the 16 GeV isolated photon sample, located in the silo and compared those results to monte carlo studies using two different fragmentation models. The results were consistent in all cases. The result quoted here for the QCD background is the result from the P16 studies, which is not subject to the vaguaries of jet fragmentation model dependence. The largest deviation in the monte carlo results from the P16 result came from the VECBOS-HERWIG study, and was included in the systematic error. We refer the reader to CDF note 2229 for the details of these studies. Of particular note is that there is a strong P_T dependence to the background relative to the signal. For example, events with $P_T < 10GeV$ have a far higher probability of being background than events above 10 GeV. Unfortunately, much of the signal also consists of low energy photons, so that the P_T cut cannot be set arbitrarily high without greatly increasing the statistical error. The integrated background numbers are summarized in Table 6.

	Run # Event #	E_T^γ (GeV)	Q_W (e)	M_T^W (GeV/c^2)	M_{CT}^W (GeV/c^2)	$\Delta R_{e\gamma}$
1	46492 – 143036	13.64	−1	82.9	92.0	1.41
2	46602 – 12455	8.82	1	76.9	88.4	2.35
3	41512 – 39510	9.73	−1	64.8	77.2	.88
4	46678 – 228687	12.45	−1	62.6	79.1	2.11
5	46655 – 360740	17.39	−1	58.9	83.5	.95
6	46655 – 691423	12.35	−1	72.0	85.2	.94
7	46680 – 481618	7.04	1	44.0	52.9	1.47
8	47008 – 165492	10.98	−1	57.9	69.2	.73
9	42490 – 54173	7.80	1	65.0	73.2	.72
10	42640 – 116172	16.14	−1	63.3	79.4	1.63
11	42743 – 14958	7.85	−1	66.7	76.0	1.06
12	42838 – 263777	18.40	−1	74.7	99.1	2.62
13	43639 – 14483	14.75	−1	140.1	157.2	.75
14	43655 – 303807	7.16	1	49.3	57.4	1.20
15	47615 – 137022	14.42	1	51.8	70.1	1.12
16	45018 – 31099	7.26	1	45.3	52.5	1.05
17	45199 – 16034	12.88	−1	62.6	77.4	1.07
18	45731 – 124780	13.51	−1	70.3	92.7	3.20
19	45754 – 89876	13.87	1	52.7	70.1	.71

Table 2: Kinematic Properties of Electron $W\gamma$ Candidates.

	Run # Event #	E_T^γ (GeV)	Q_W (e)	M_T^W (GeV/c^2)	M_{CT}^W (GeV/c^2)	$\Delta R_{\mu\gamma}$
1	41449 – 14966	8.63	1	55.2	68.9	1.19
2	41771 – 89497	24.13	1	62.2	99.5	3.11
3	43048 – 137910	18.47	−1	43.9	65.6	1.60
4	45069 – 14121	8.72	−1	42.4	55.3	2.56
5	45878 – 99890	7.31	−1	73.5	89.1	2.06
6	46935 – 173074	9.06	1	54.7	66.4	2.86
7	47814 – 4246	11.81	−1	121.1	143.1	1.17

Table 3: Kinematic Properties of Muon $W\gamma$ Candidates.

	Run # Event #	E_T^γ (GeV)	$M_{e^+e^-}$ (GeV/c^2)	$M_{Z\gamma}$ (GeV/c^2)	$\Delta R_{e\gamma}$
1	42213 – 53208	7.04	89.1	97.0	.91
2	42821 – 178009	8.31	85.8	95.2	1.40
3	47552 – 126373	8.04	91.8	102.7	1.67
4	45305 – 49392	23.69	92.3	114.3	1.57

Table 4: Kinematic Properties of Electron $Z\gamma$ Candidates.

	Run # Event #	E_T^γ (GeV)	$M_{\mu^+\mu^-}$ (GeV/c^2)	$M_{Z\gamma}$ (GeV/c^2)	$\Delta R_{\mu\gamma}$
1	42727 – 30958	9.32	88.5	101.1	1.80
2	45610 – 147664	63.58	87.7	188.4	2.86
3	46170 – 87849	12.79	91.6	110.5	2.40
4	46655 – 256640	10.80	72.8	88.7	0.98

Table 5: Kinematic Properties of Muon $Z\gamma$ Candidates.

Jet background		
W samples	Electron	Muon
P16 ($\Delta R_{JJ} > 1.4$)	$4.6 \pm 1.1 \pm 1.5$	$1.9 \pm 0.5 \pm 0.6$
VecBos ($\Delta R_{\ell J} > 0.7$)	3.5 ± 1.3	1.9 ± 1.1
Z samples	Electron	Muon
P16 ($\Delta R_{JJ} > 1.4$)	$0.4 \pm 0.1 \pm 0.2$	$0.1 \pm 0.03 \pm 0.04$
VecBos ($\Delta R_{\ell J} > 0.7$)	0.3 ± 0.1	0.1 ± 0.1

Table 6: QCD γ Background Estimates

4 Other Backgrounds

$Z\gamma$ and inclusive Z+jet processes (where the QCD jet fakes a photon) could contribute to $W\gamma$ background (particularly in the muon channel) when one of the leptons from the $Z-$decay is not detected, resulting in the (one-legged) Z being mis-identified as a W. For electron/muon $W\gamma$ candidate events, contamination from one-legged $Z\gamma$ events was suppressed in each sample by making a "no 2^{nd} track" cut for 3-D tracks with $P_T > 10\ GeV/c$ outside of hadronic jets (EM fraction < 0.85). If the 2^{nd} track was *not* pointing at a jet and has a pair-mass(with the charged lepton from the W) of $70 < M_{ee} < 110$ ($40 < M_{\mu\mu} < 140$) for electrons (muons), the event was rejected as a one-legged $Z\gamma$ candidate, as listed in section 2. For muons, the 2^{nd} track was also required to have a minimum-ionizing calorimeter signature. From studies using QFL $W\gamma$ MC simulated data for electrons and muons, no signal events were lost by these 2^{nd} track-type cuts. The contributions to the $W\gamma$ background from these processes were estimated using inclusive Z data and the Baur $W\gamma$ and $Z\gamma$ Monte Carlo programs. These results are summarized in Table 7 below. We note here that one electron 1-legged $Z\gamma$ candidate was found in the electron $W\gamma$ data sample (~ 0.7 events expected), and no 1-legged $Z\gamma$ candidates were found in the muon $W\gamma$ data sample (~ 1.2 events expected).

The processes $(W \to \tau\nu_\tau) + \gamma$ and $(W \to \tau\nu_\tau)$ + Jet also contributed to the background in the electron and muon $W\gamma$ data samples when the τ decayed to an electron or muon, respectively. The corresponding processes $(Z \to \tau^+\tau^-) + \gamma$ and $(Z \to \tau^+\tau^-)$ + Jet also contributed to the background in the electron and muon $Z\gamma$ data samples. The tau decay contribution to the $W\gamma$ background in the electron and muon channels, was determined using

Background Process	Electron	Muon
$Z+\gamma \rightarrow$ "$W+\gamma$": w/ 2^{nd} Leg Cut	0.5 ± 0.1	1.2 ± 0.1
$(W \rightarrow \tau\nu_\tau, \tau \rightarrow \ell\nu_\ell\nu_\tau)+\gamma$	0.3 ± 0.03	0.2 ± 0.02

Table 7: Additional Backgrounds to e and μ

the Baur generator and the fast detector simulation and was found to be 0.3 and 0.2 events, respectively, as shown in table 7. The tau decay contribution to the $Z\gamma$ background in the electron and muon channels was found to be extremely small owing to our dilepton pair mass cut ($<<$ 1 events), and hence is neglected.

A summary of the backgrounds for each of the four data samples can be found in table 13, together with the number of observed and expected events. The first uncertainty in each table entry is the statistical uncertainty; where there is a second uncertainty in the background number it is the systematic uncertainty on the determination of the QCD jet-faking photon background for that channel. We conservatively defined this error as the difference between the QCD background as determined from the P16 data and the QCD background as determined from the Vecbos/HERWIG/QFL $W/Z+n-$jets MC simulations.

5 Photon Efficiencies

The overall efficiency for CEM photons was determined from the product of efficiencies associated with the CEM photon cuts described in section 2. The efficiency for the calorimeter isolation in a cone of $\Delta R = 0.4$ ($ET4/E_T$) in the central calorimeter ($|\eta| < 1.1$) was measured using random cones in the inclusive W/Z data samples. Five random cones were thrown in each event, and the cone of $\Delta R = 0.4$ was required to be more than $\Delta R = 0.7$ away from the W/Z decay lepton(s). The calorimeter energy in the cone was clustered to get the $\sum E_T$. CTC tracks in the cone were used to get the $\sum P_T$ and number of 3-d tracks pointing to the cluster. The procedure for determining the efficiency for a random cone with $ET(X) < ET4 < ET(X + .25GeV)$ was done by counting events in each ET4 bin(of .25 GeV) from $X = 0to10.0$ Gev. From that distribution we determine the efficiency for $\sum E_T < X$ by summing the contents of all bins up to X and dividing the sum by the total number of random cones. We then get the efficiency for $ET4/E_T < 0.15$ as a function of photon E_T. For example, for a photon with $E_T = 10GeV$ the requirement is that the $\sum E_T < 1.5$. The isolation efficiency is then calculated using the weighted averages of the photon P_T distribution. The result, shown in table 8, is that the E_T dependence varies from about 90% for low energy photons up to nearly 100% for photons with $E_T > 25GeV$. As we observed in our previous note, an independent study of efficiency losses in Minimum Bias and Jet 20 events lead to results which differ by as much as 6 percent with the ones obtained in the study with $W+$ jet events. This can be explained by the different underlying event structure in IVB + jet events, Minimum Bias and QCD jet events. We expect

$ETBin(GeV)$	$\epsilon_{ET4/ET<0.15}$
7-11	$89.2 \pm 1.0\%$
11-15	$94.2 \pm 1.0\%$
15-19	$96.5 \pm 1.0\%$
19-23	$97.6 \pm 1.0\%$
23-27	$98.3 \pm 1.0\%$
27-10000	$99.1 \pm 1.0\%$

Table 8: E_T dependent CEM photon isolation efficiency.

Data Sample	$\epsilon_{\Sigma PT4<2.0\cdot N3d}$	
W_e Random Cones	$90.8 \pm 0.2\%$	
W_μ Random Cones	$90.8 \pm 0.2\%$	

Table 9: CEM photon efficiencies

that soft particle multiplicities in the underlying events which cause inefficiencies in isolation cuts, are higher, the more inelastic the collision is and the more jet activity the event has, and therefore the efficiency estimates for IVB + photon events should lie in between the ones obtained in IVB + Jet events and *all* IVB events. Since, however, the photons in our analysis are comparably soft, we regard it a justified approximation to base our efficiency determination on our IVB event sample.

The efficiencies for the summed P_T in a cone of $\Delta R = 0.4$, $(\sum PT4)$ downstream of the $ET4$ cut(s) for CEM photons and for the "No 3D CTC Track" pointing at the CEM cluster (N3D=0) were also determined from these same data samples, and the results are shown in table 9. These photon efficiencies, obtained from random cones thrown in both the electron and muon inclusive W/Z data samples, are in good agreement with one another.

The efficiencies for $Had/EM < 0.055 + 0.00045 * E$, $L_{shr} < 0.5$, $\chi^2_{\rm strip} < 20.0$ and $\chi^2_{\rm wire} < 20.0$ and the no 2^{nd} CES strip/wire cluster $E_{CES\ 2^{nd}} > 1\ GeV$ cuts were determined from $5 - 50\ GeV$ CEM electron test beam data. The efficiency for the non-P_T dependent isolation cuts, the cuts above, the photon conversion efficiency and the different e-γ shower development combine to give an efficiency of $81.2 \pm 1.3 \pm 1.9\%$. This common efficiency was used with the E_T dependent isolation efficiency to determine the overall photon efficiency. The efficiencies for these photon cuts for CEM photons, and the overall CEM photon efficiency, are summarized in Tables 10-12.

The isolation and overall CEM photon efficiencies are plotted as a function of photon E_T in figure 7. The efficiencies listed in table 12 are just the weighted averages of the efficiencies plotted in figure 7.

The overall photon efficiency was lower in our present data sample than in the 1988/1989

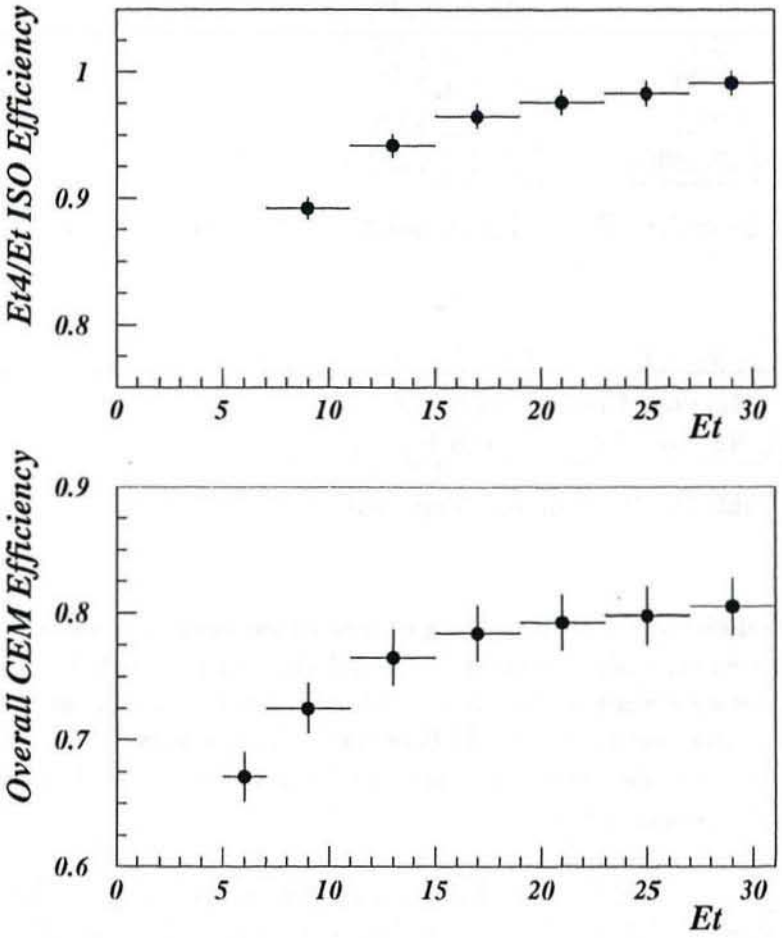

Figure 7: CEM photon isolation(top) and overall(bot) efficiency as a function of Et.

Data Sample	$\epsilon^{\gamma}_{Had/EM}$	ϵ^{γ}_{Lshr}	$\epsilon^{\gamma}_{\chi^2_{stp}+\chi^2_{wir}}$	$\epsilon^{\gamma}_{no\ 2^{nd}\ CES}$
5 GeV e Test Beam	$98.9 \pm 0.2\%$	$99.9 \pm 0.1\%$	$97.3 \pm 0.3\%$	$98.0 \pm 0.1\%$
10 GeV e Test Beam	$99.6 \pm 0.1\%$	$98.8 \pm 0.4\%$	$96.2 \pm 0.4\%$	$97.9 \pm 0.1\%$
18 GeV e Test Beam	$99.1 \pm 0.9\%$	$100.0\ ^{+0.0}_{-1.7}\%$	$98.2 \pm 1.8\%$	$98.2 \pm 1.6\%$
30 GeV e Test Beam	$98.9 \pm 0.9\%$	$100.0\ ^{+0.0}_{-1.1}\%$	$99.2 \pm 0.7\%$	$98.2 \pm 1.0\%$
50 GeV e Test Beam	$98.0 \pm 0.3\%$	$99.9 \pm 0.1\%$	$99.2 \pm 0.2\%$	$97.6 \pm 0.2\%$

Table 10: CEM Photon Efficiency Determination – EM Shower Variables. The statistical uncertainty associated with each quantity is given.

$\epsilon^{\gamma}_{\Sigma PT4}$	$95.2 \pm 0.1 \pm 0.8\%$	Tracking Isolation
ϵ^{γ}_{N3D}	$95.6 \pm 0.1 \pm 0.7\%$	No track @ EM Cluster
$\epsilon^{\gamma}_{Had/EM}$	$99.2 \pm 0.9 \pm 0.8\%$	Had/EM Cut
ϵ^{γ}_{Lshr}	$99.9 \pm 0.1 \pm 0.3\%$	Lateral Shower Cut
$\epsilon^{\gamma}_{\chi^2_{stp}+\chi^2_{wir}}$	$98.4 \pm 0.1 \pm 0.9\%$	CES strip/wire χ^2 Cut
$\epsilon^{\gamma}_{no\ 2^{nd}\ CES}$	$97.9 \pm 0.7 \pm 1.0\%$	No 2^{nd} CES Clusters
$\mathcal{P}^{\gamma}_{\overline{conv}}$	$93.4 \pm 0.1 \pm 0.5\%$	Photon Survival
$\mathcal{S}^{cem}_{e\rightarrow\gamma}$	$100.3 \pm 0.6 \pm 1.0\%$	e *vs.* γ Shower Development
ϵ^{γ}_{cem}	$81.2 \pm 1.3 \pm 1.9\%$	Overall Photon Efficiency

Table 11: Overall CEM Photon Efficiency Determination. The statistical and sytematic uncertainties associated with each quantity are given.

Data Sample		
W_e Random Cones	$75.2 \pm 2.1\%$	
W_μ Random Cones	$75.3 \pm 2.1\%$	
Z_μ Random Cones	$76.8 \pm 1.7\%$	

Table 12: Overall CEM Photon Efficiency- weighted average over P_T bins.

Channel	N_{obs}	$\sum N_{bkgnd}$	N_{signal}	N_{pred}^{SM}
$e\ W\gamma$	19	$5.4 \pm 1.1 \pm 1.5$	$13.6 \pm 4.5 \pm 3.5$	$17.0 \pm 1.8 \pm 2.3$
$\mu\ W\gamma$	7	$3.3 \pm 0.5 \pm 0.6$	$3.7 \pm 2.6 \pm 0.6$	$8.6 \pm 0.9 \pm 1.7$
$e\ Z\gamma$	4	$0.4 \pm 0.1 \pm 0.2$	$3.6 \pm 2.0 \pm 1.8$	$4.7 \pm 0.5 \pm 0.5$
$\mu\ Z\gamma$	4	$0.1 \pm 0.03 \pm 0.04$	$3.9 \pm 2.0 \pm 1.6$	$3.1 \pm 0.3 \pm 0.3$

Table 13: Summary of $W\gamma$ and $Z\gamma$ Results

data. This is caused by the higher average luminosities in the 1992/1993 running, where the probability of multiple interactions was higher. Another, smaller effect is the higher photon conversion rate, caused by the greater amount of material in the detector.

6 Comparisons to Monte Carlo Predictions

To simulate our observed data, generate kinematic distributions and calculate acceptances, we used two complementary Monte Carlo methods, as described in CDFR 1941. One simulation program used a "fast" parameterization of the detector, the second used the more detailed QFL structure, which required more computing time. As an event generator, both simulations used the Baur $W\gamma$ and $Z\gamma$ Monte Carlo programs for generation of electron, muon and tau $W\gamma$ and $Z\gamma$ MC data samples [5]. The Baur + QFL simulation [6] used unweighted IVB + photon events and included an underlying event generated by ISAJET.

We generated events using MRSD-' [7] structure functions, which best match the CDF charge asymmetry measurements in W decays [8] and also recent data from Hera. We used other structure function sets to measure systematic errors, see section 7.

The number of electron and muon $W\gamma$ and $Z\gamma$ candidates are summarized in Table 13 together with our background estimate, the background-subtracted signal and the Monte Carlo expectation.

The data are in agreement with Standard Model expectations, although there are a lower number of events in the muon channel than expected. Figure 8 shows the photon E_T distribution in the combined electron and muon W samples, compared to the Monte Carlo prediction of signal plus background. Figure 9 shows the separation in ΔR between the charged lepton and photon. The transverse cluster mass for the combined e and μ W samples is shown in figure 10. The background distributions were taken directly from the P16 data for the E_T plot, and for the other figures, the background shape was taken from the W

+ jet simulations and scaled to the P16 value. We observe that the distributions are in good agreement with Standard Model predictions and note there is no excess of high transverse momentum photons, the presence of which would indicate new physics. The distributions also show that a significant contribution to our photon signal is from radiative W decays. The transverse cluster mass is defined as

$$M_{CT}^{W} = [(M_{l\gamma}^{2} + |\mathbf{P_T^{\gamma}} + \mathbf{P_T^{l}}|^{2})^{\frac{1}{2}} + |\mathbf{P_T^{\not\nu}}]^{2} - |\mathbf{P_T^{\gamma}} + \mathbf{P_T^{l}} + \mathbf{P_T^{\not\nu}}|^{2}$$

where $M_{l\gamma}^{2}$ is the invariant mass of the lepton-photon system. If an additional cut on the cluster transverse mass of $M_{CT}^{W} \geq 90\ GeV/c^{2}$ is applied, 6 out of 26 e+μ events survive. Two of these events, with large transverse mass *and* large transverse cluster mass in figure 10 are particularly unusual. Figure 11 shows the photon E_T distribution in the combined electron and muon Z samples, compared to the Monte Carlo prediction of signal plus background. Figure 12 shows the lepton-lepton-photon mass in the combined electron and muon Z samples, compared to the Monte Carlo prediction of signal plus background. Within the limited statistics the agreement appears good, although there is an interesting event in the muon sample with photon $E_T > 60\ GeV$ that is also somewhat unexpected. It is also interesting to note that 7 of the 8 events in the combined Z samples have a 3-body mass greater than 95 GeV.

7 Systematic Errors

We used the fast detector simulation on Baur monte carlo data to obtain Standard Model cross sections and the predicted number of events. These results can vary systematically according to the choice of structure function, Q^2, and the magnitude of the Pt boost applied to the system. Studies have been done for all four samples, using five structure function choices, three choices of Q^2, and three choices of P_T boosting. In each case the nominal value for two of the three variables was kept fixed while the third was varied. The P_T boost of the $W\gamma$ system was varied within the uncertainty in the shape of the W P_T distribution measured by CDF [9]. This seems reasonable given the results of the study published by Baur, Han and Ohnemus [10] which finds very little effect of higher order QCD corrections to the P_T distribution of photons in W-photon events. The structure functions used were HMRSB, MRS S0', MRS D0', MRS D-' (default), and CTEQ 2pM, while the Q^2 choices were $M_{lV B\gamma}^{2}/4$, $M_{lV B\gamma}^{2}$ (default), and $4M_{lV B\gamma}^{2}$.

Typically, the effect each choice has on the Standard Model prediction of the number of events per E_T bin is small. The structure function choice has about a 10-15% effect on the number of predicted events while Q^2 and the P_T boosting give 5-10% variations in the number of predicted events across all E_T bins. When all the variations are added in quadrature the overall effect on the Standard Model total number of events and cross section is about 15% for each channel. The results of these studies are shown in tables 14 and 15. Note that for the $W\gamma$ case the difference between the number of predicted events from the two Monte Carlo methods is included in the overall systematic error.

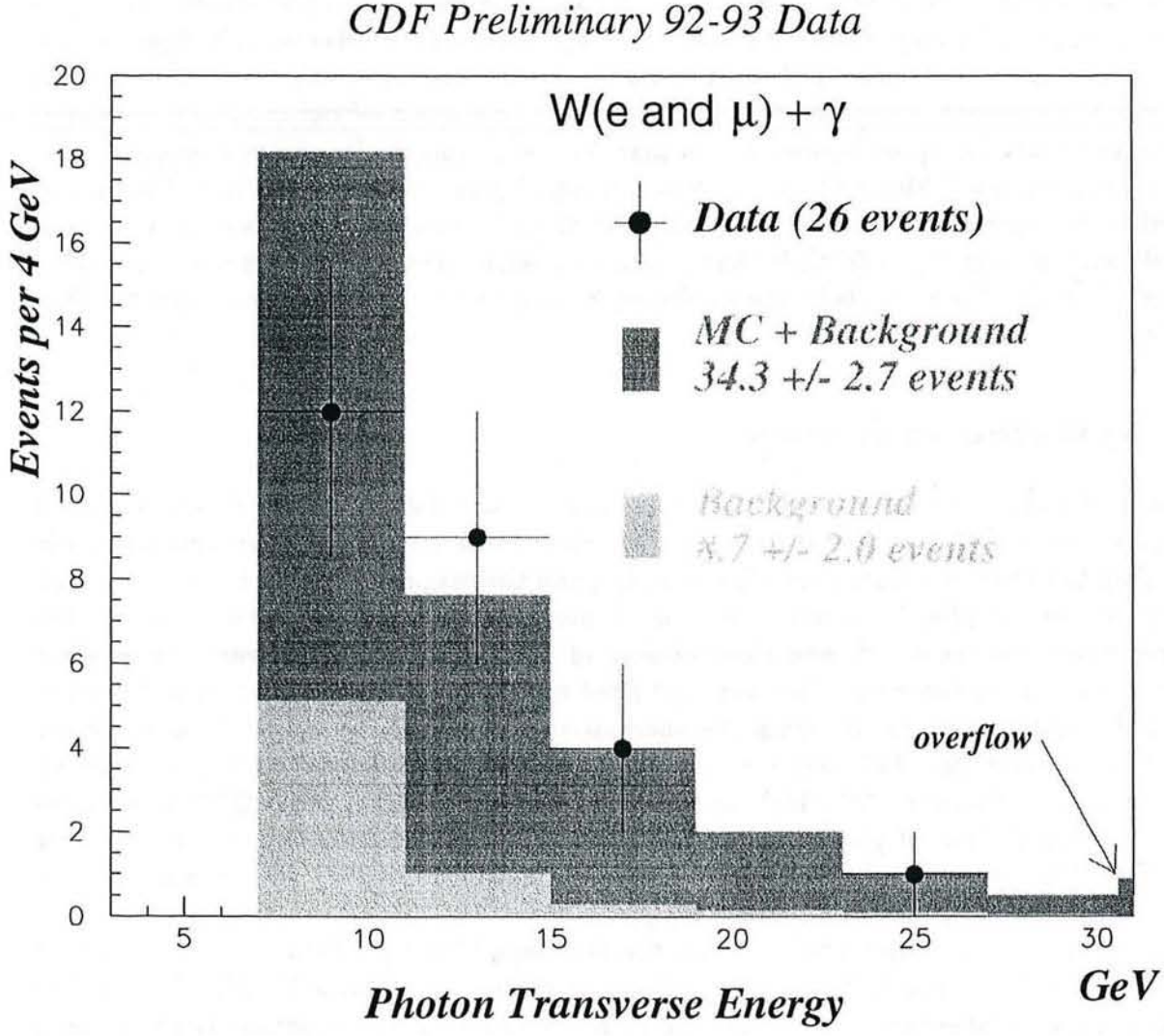

Figure 8: Et of the W photon candidates

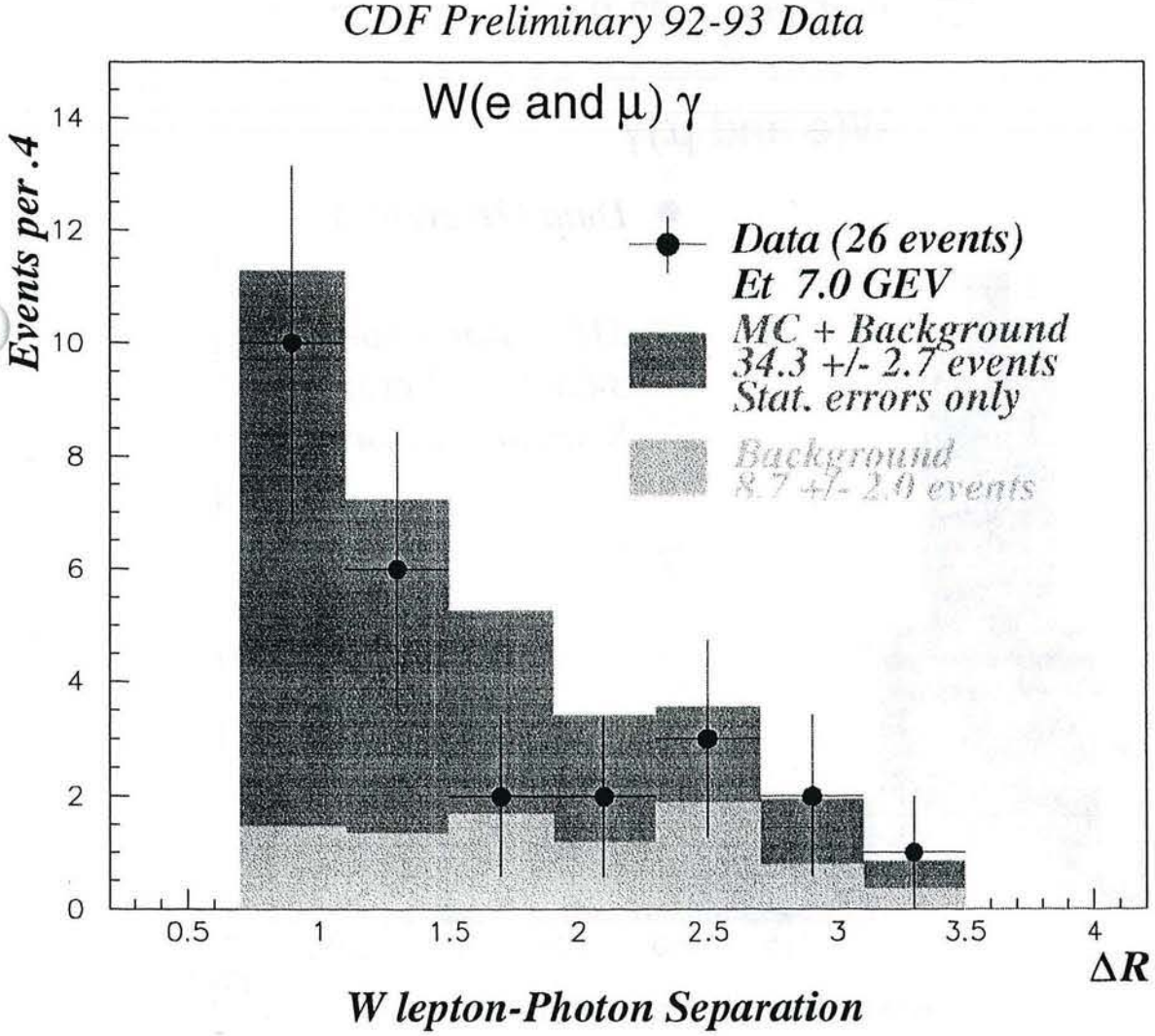

Figure 9: Separation in Delta R of the photon candidate and the charged lepton from the W decay.

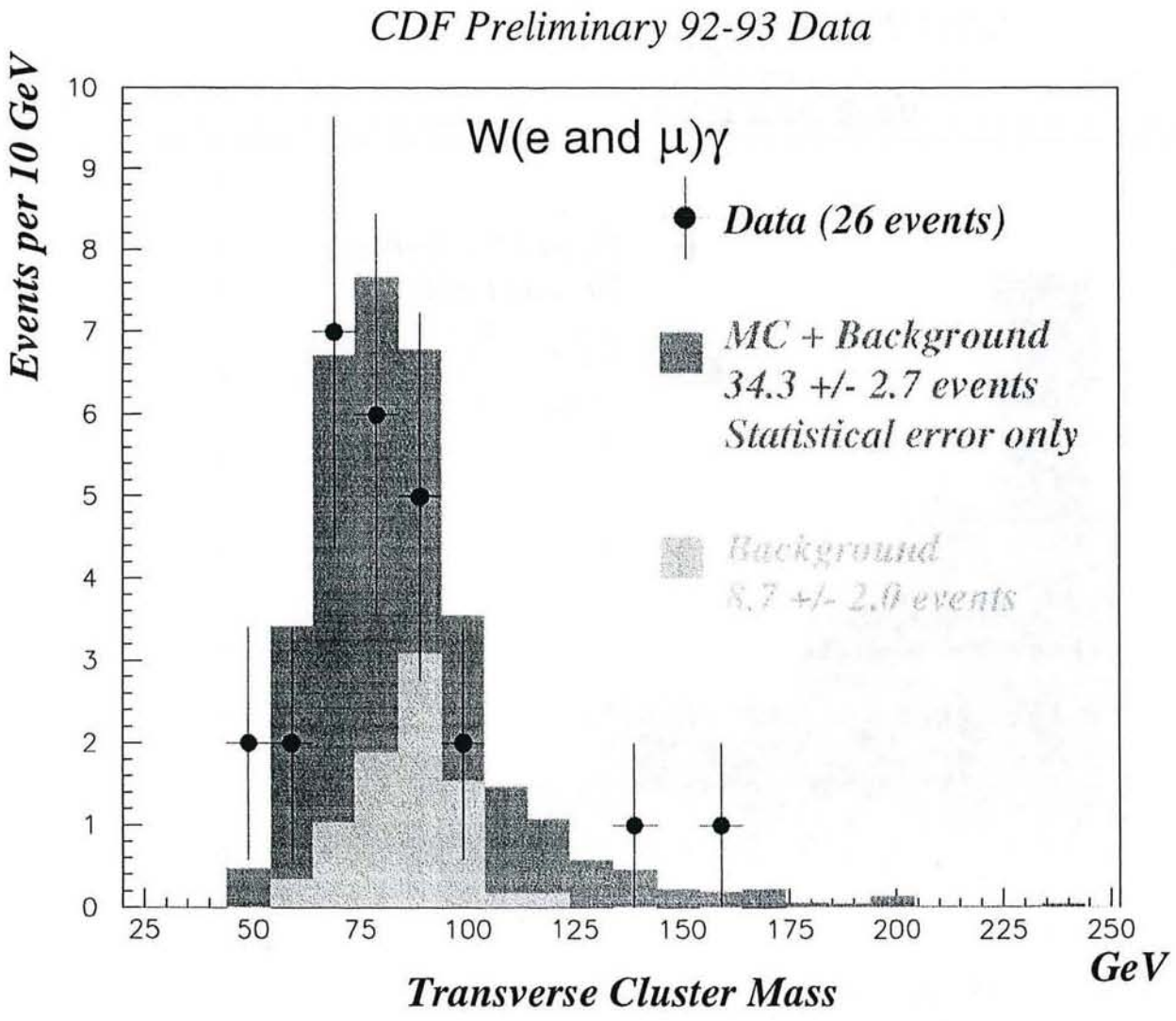

Figure 10: Transverse cluster mass of the W leptons and the photon.

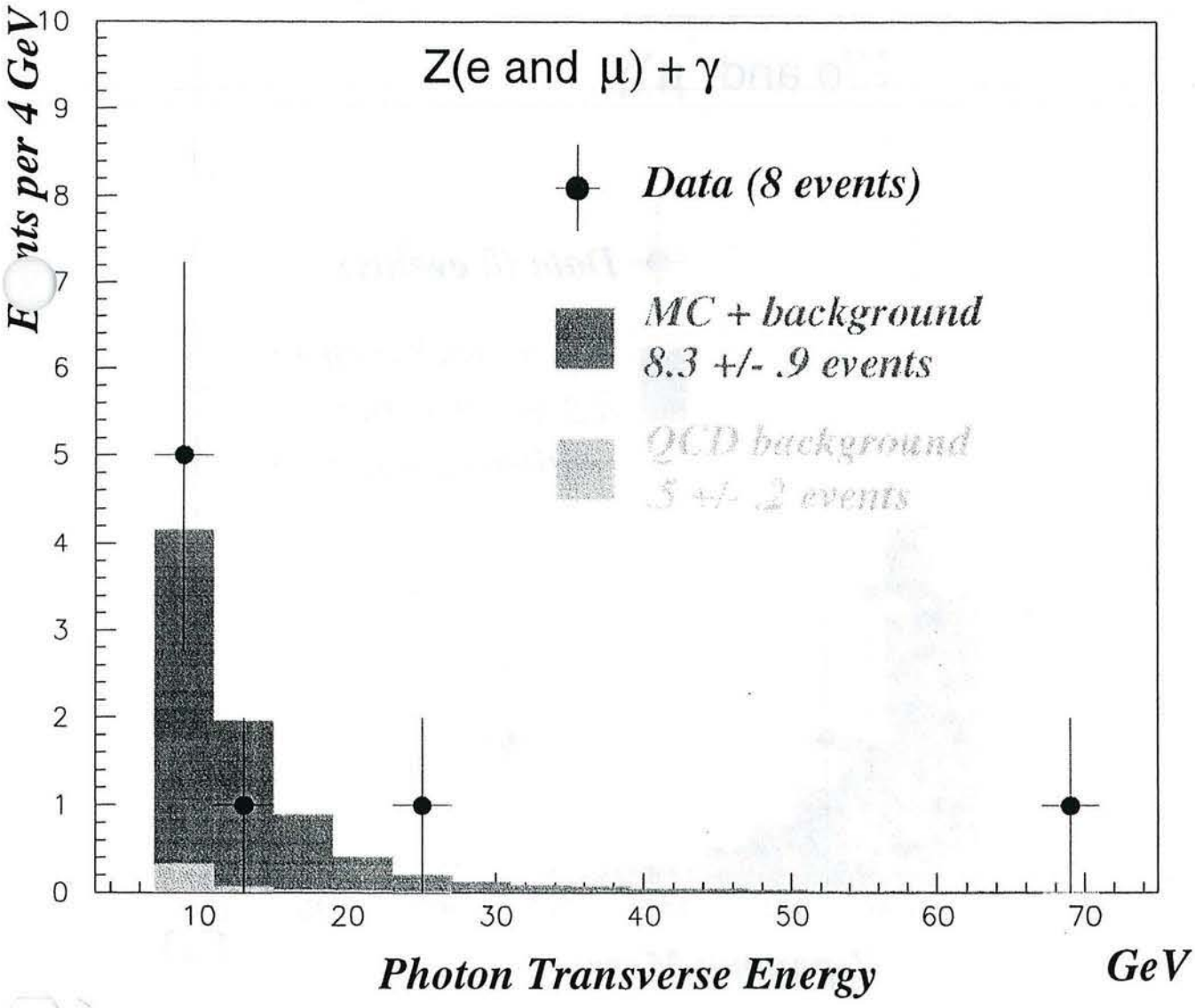

Figure 11: Et of the Z photon candidates

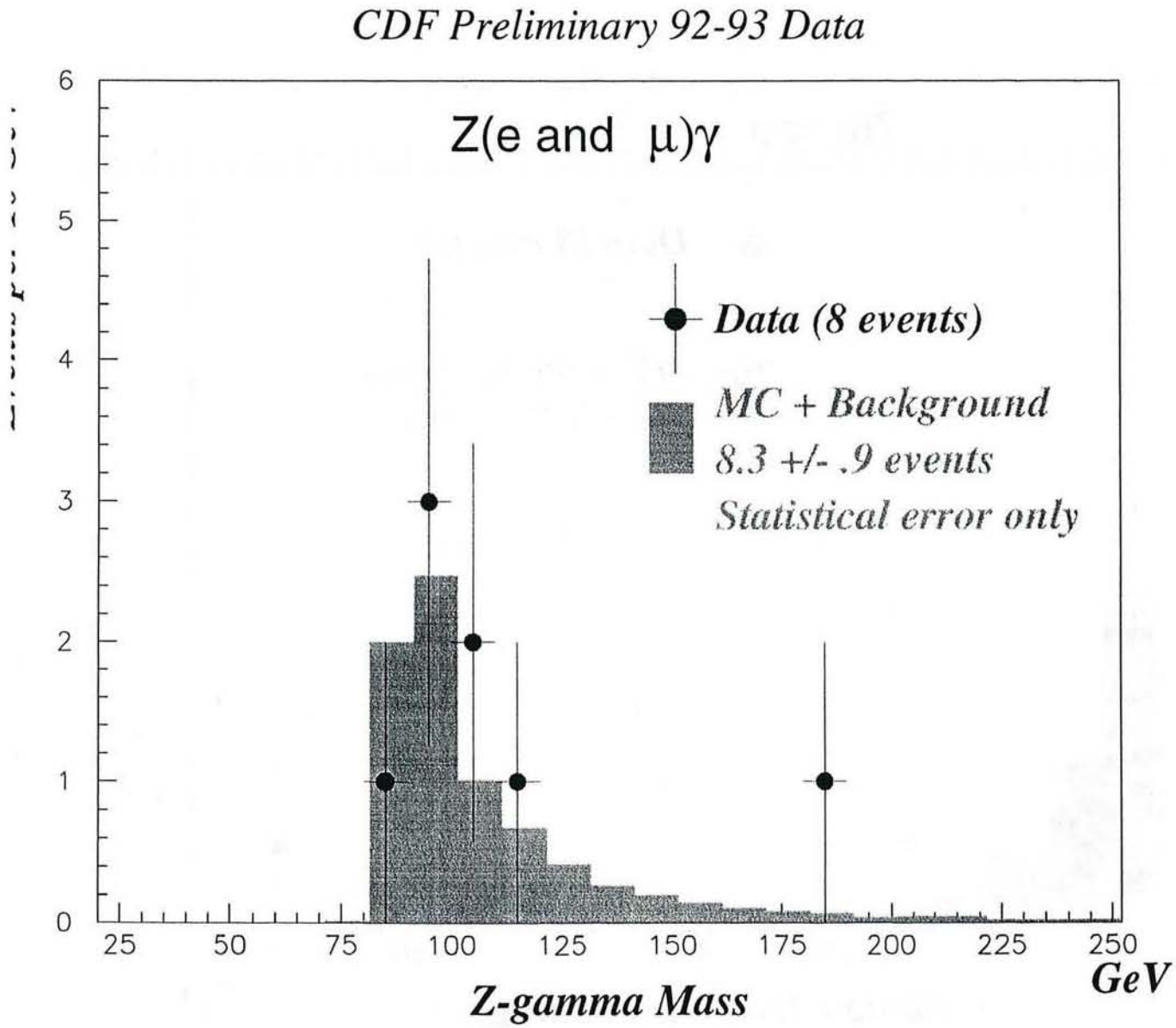

Figure 12: Mass of the Z photon candidates

8 $\sigma * BR(W+\gamma)$ and $\sigma * BR(Z+\gamma)$

The experimental results for the cross sections × branching ratios for $W\gamma$ and $Z\gamma$ in the electron/muon channels were determined from the number of observed events minus the estimated number of background events, corrected for all acceptances and efficiencies, and divided by the integrated luminosity :

$$\sigma_W \cdot B(W \to \ell\nu_\ell\gamma) = \frac{\mathcal{N}^{W\gamma}_{observed} - \sum \mathcal{N}^{W\gamma}_{background}}{A_{W\gamma} \cdot \epsilon_{W\gamma} \cdot \int \mathcal{L}_\ell dt}$$

$$\sigma_Z \cdot B(Z \to \ell^+\ell^-\gamma) = \frac{\mathcal{N}^{Z\gamma}_{observed} - \sum \mathcal{N}^{Z\gamma}_{background}}{A_{Z\gamma} \cdot \epsilon_{Z\gamma} \cdot \int \mathcal{L}_\ell dt}$$

where $\mathcal{N}^{W\gamma}_{observed}$ and $\mathcal{N}^{Z\gamma}_{observed}$ are the number of observed $W\gamma$ and $Z\gamma$ events in a particular decay channel (e or μ); $\sum \mathcal{N}^{W\gamma}_{background}$ and $\sum \mathcal{N}^{Z\gamma}_{background}$ are the number of (summed) background events expected in each of the data samples. The product terms $A_{W\gamma} \cdot \epsilon_{W\gamma}$ and $A_{Z\gamma} \cdot \epsilon_{Z\gamma}$ are the (overall) acceptance × efficiency factors for detecting the $W\gamma$ and $Z\gamma$ events, respectively. The integrated luminosity ($\int \mathcal{L}_\ell dt$) in the denominator then normalizes the number of events to our particular data samples.

The product acceptance × efficiency terms are in fact products of a number of acceptances × efficiencies:

$$A_{W\gamma} \cdot \epsilon_{W\gamma} = A_W \cdot A^\gamma_{\rm geom} \cdot \epsilon_{\rm lepton} \cdot \epsilon_{\rm photon} \cdot \epsilon_{\rm trigger} \cdot \epsilon_{\rm Analysis\ cuts}$$

The acceptance A_W is the combined lepton fiducial, lepton & $\not\!\!E_T$ kinematic acceptance for the W boson; the acceptance $A^\gamma_{\rm geom}$ is the combined geometric and kinematic acceptance of the photon to pass through the CEM calorimeter. The ϵ terms are (product) efficiencies for detecting the lepton or the photon once they have passed through their respective detectors. The term $\epsilon_{\rm lepton}$ is the efficiency for the CEM (CMU) system to record the electron (muon) in the event, whereas $\epsilon_{\rm photon}$ is the efficiency for the calorimeters to record the passage of the photon. The term $\epsilon_{\rm trigger}$ is the lepton trigger efficiency. The term $\epsilon_{\rm Analysis\ cuts}$ is itself a product of efficiencies of the cuts used to make the data sample, e.g. electron/muon isolation. Tables 16 - 18 summarize the acceptances determined from the fast MC detector simulation(s) for the 92/93 data samples. Tables 19 - 21 show the electron and muon efficiencies calculated for the 92/93 data.

Effect	Ele. Events	Ele. $\sigma \cdot BR$	Muon Events	Muon $\sigma \cdot BR$
SF	1.84	2.34 pb	1.14	2.33 pb
Pt Boost	0.93	1.63 pb	0.65	1.62 pb
Q^2	0.67	0.18 pb	0.06	0.18 pb
QFL - FMC	0.8	—	1.1	—
Sum in Quadrature	2.31	2.86 pb	1.71	2.84 pb

Table 14: Fast Monte Carlo Systematics in 92/93 e and μ $W\gamma$ Samples

Effect	Ele. Events	Ele. $\sigma \cdot BR$	Muon Events	Muon $\sigma \cdot BR$
SF	0.51	0.58 pb	0.25	0.58 pb
Pt Boost	0.09	0.09 pb	0.04	0.09 pb
Q^2	0.10	0.10 pb	0.03	0.09 pb
Sum in Quadrature	0.52	0.59 pb	0.27	0.59 pb

Table 15: Fast Monte Carlo Systematics in 92/93 e and μ $Z\gamma$ Samples

The cross section results for each of the four channels are summarized in Table 22 for $W\gamma$ and $Z\gamma$. The first error is the statistical error, and the second error is the systematic error, coming mainly from the QCD photon background determination and a $\pm 10\%$ error associated with the integrated luminosity. The measured values for the W electron and Z cases agree reasonably well with the standard model predictions. The W electron case is less than one sigma lower than the prediction, and the average of the Z cases is very close to the standard model prediction. The muon W sample is roughly two sigma below the predicted value, and for this we have no explanation. The sample was studied carefully for effects that could cause us to lose events, but none were found, and we have been forced to conclude that it is a statistical fluctuation.

Acceptance	Electron	Muon
A_W	$20.10 \pm 0.02\%$	$11.84 \pm 0.02\%$
A_Z	$28.57 \pm 0.07\%$	$13.45 \pm 0.05\%$
A_{oo}	$12.76 \pm 0.05\%$	$4.22 \pm 0.03\%$
A_{ox}	$13.18 \pm 0.05\%$	$9.24 \pm 0.04\%$
A_{oy}	$2.62 \pm 0.02\%$	$- - -$
A_{ZW}	$9.87 \pm 0.04\%$	$16.24 \pm 0.05\%$

Table 16: 92/93 W and Z Acceptances for e and μ $W\gamma$ and $Z\gamma$

$W\gamma$	Electron	Muon
f'^{γ}_{cem}	$47.69 \pm 0.20\%$	$47.62 \pm 0.20\%$
A'^{γ}_{cem}	$76.45 \pm 0.55\%$	$75.93 \pm 0.73\%$

Table 17: 92/93 Photon Acceptances for e and μ $W\gamma$

$Z\gamma$	Electron	Muon
f^{γ}_{coo}	$9.00 \pm 0.16\%$	$3.01 \pm 0.01\%$
f^{γ}_{cox}	$12.30 \pm 0.18\%$	$8.88 \pm 0.16\%$
f^{γ}_{coy}	$3.18 \pm 0.01\%$	$0.0 \pm 0.0\%$
A^{γ}_{coo}	$76.40 \pm 0.09\%$	$76.44 \pm 0.16\%$
A^{γ}_{cox}	$75.66 \pm 0.09\%$	$76.61 \pm 0.09\%$
A^{γ}_{coy}	$78.29 \pm 0.37\%$	$0.0 \pm 0.0\%$

Table 18: 92/93 Photon Acceptances for e and μ $Z\gamma$

$\mathcal{L}_e \cdot dt$	$21.7 \pm 2.2\ pb^{-1}$	Integrated Luminosity
ϵ_{zvx}	0.960 ± 0.003	$\lvert Z_{vtx}\rvert < 60\ cm$
ϵ^{CEM}_{iso}	0.973 ± 0.005	Electron Isolation (R=0.4)
$\epsilon^{CEM}_{Had/EM}$	1.000 ± 0.005	$Had/EM < ABW$
$\epsilon_{\chi^2_{stp}}$	0.950 ± 0.007	$\chi^2_{stp} < 15$
$\epsilon^{CEM}_{L_{shr}}$	0.980 ± 0.004	$L_{shr} < 0.2$
$\epsilon_{E/P}$	0.950 ± 0.007	$.5 <$ CEM E/P < 2.0
ϵ^{CEM}_{trk}	1.000 ± 0.001	CTC Tracking
ϵ^{CEM}_{dz}	0.982 ± 0.004	$dz < 3.0\ cm$ Matching Cut
ϵ^{CEM}_{dx}	0.941 ± 0.008	$dx < 1.5\ cm$ Matching Cut
$T = \epsilon_{L1} \cdot \epsilon_{L2} \cdot \epsilon_{L3}$	0.952 ± 0.003	Fiducial Electron Trigger

Table 19: Electron Efficiencies for $W\gamma$ and $Z\gamma$

$\mathcal{L}_\mu \cdot dt$	$20.6 \pm 2.1 pb^{-1}$	Integrated Luminosity
ϵ_{cmudx}	0.973 ± 0.008	CTC-CMU Track-Stub Match
ϵ_{cmpdx}	$0.998 + 0.002 - 0.005$	CTC-CMP Track-Stub Match
ϵ_{em}	$0.969 + 0.006 - 0.007$	EM Energy in Muon Tower
ϵ_{had}	$0.989 + 0.004 - 0.005$	EM Energy in Muon Tower
ϵ_{iso}	$0.957 + 0.008 - 0.009$	Muon Border Tower Energy
ϵ_{cos}	0.997 ± 0.002	Cosmic Ray Filter
ϵ_{L1}	0.93 ± 0.01	Level-1 Trigger
ϵ_{L2}	0.97 ± 0.01	Level-2 Trigger
ϵ_{L3}	0.98 ± 0.01	Level-3 Trigger
$T = \epsilon_{L1} \cdot \epsilon_{L2} \cdot \epsilon_{L3}$	0.87 ± 0.02	Fiducial Muon Trigger

Table 20: Muon Efficiencies for $W\gamma$ and $Z\gamma$

Acceptance × Efficiency Factor	Electron	Muon
$A^{\ell}_{W\gamma} \cdot \epsilon^{\ell}_{W\gamma}$	$4.2 \pm 0.1\%$	$2.3 \pm 0.1\%$
$A^{\ell}_{Z\gamma} \cdot \epsilon^{\ell}_{Z\gamma}$	$4.7 \pm 0.2\%$	$3.0 \pm 0.1\%$

Table 21: Overall Acceptances × Efficiency Factors for Electron and Muon $W\gamma/Z\gamma$.

Channel	$\sigma \cdot B_{expt}$ (pb)	$\sigma \cdot B^{SM}_{pred}$ (pb)
e $W\gamma$	$14.9 \pm 5.0 \pm 4.1$	$18.6 \pm 0.1 \pm 2.9$
μ $W\gamma$	$8.0 \pm 5.6 \pm 1.5$	$18.5 \pm 0.1 \pm 2.8$
e $Z\gamma$	$3.5 \pm 2.0 \pm 1.8$	$4.8 \pm 0.02 \pm 0.6$
μ $Z\gamma$	$6.3 \pm 3.3 \pm 2.7$	$4.8 \pm 0.02 \pm 0.6$

Table 22: Summary of $\sigma * BR(W + \gamma)$ and $\sigma * BR(Z + \gamma)$ Results.

9 Limits on Anomalous Couplings and Moments

The presence of anomalous couplings in IVB - photon couplings would imply the lack of full gauge cancellations at high energies. As a result we would observe an increase of the cross section of IVB - photon couplings with the center of mass energy of the IVB + Photon system, displaying the onset of new physics such as compositeness, without which the cross section would rise beyond the unitarity limit. In our detector this effect would manifest itself in a pronounced tail in the P_T gamma distribution which would lead to an enhancement of the IVB + photon cross section compared to SM expectation.

In our analysis of the '89 data, the measured cross section times branching ratio for W/Z + photon production was consistent with the SM expectation, but the large statistical and systematical uncertainties left room for sizeable deviations from the SM. We extracted limits on anomalous couplings from limits on possible upward fluctuations of our measured cross sections. We find consistency with SM predictions in the 92/93 data also, as has been shown earlier in this note. In particular we do not find excess events in the tails of our photon P_T distributions. For a more sensitive determination of limits on possible anomalous couplings we analysed the photon P_T distribution and compared it with Monte Carlo predictions for SM or anomalous couplings. The Monte Carlo generator is the Baur generator, and the detector simulation is performed with the Fast Monte Carlo. We added bin-by-bin to the simulated IVB gamma signal all sources of background as described earlier (see Figure 8) . For each P_T bin we calculated the likelihood that our simulated measurement would fluctuate to our observed number of events. Since we have only small event numbers in each bin, these probabilities are governed by Poisson statistics. The probabilities for all bins are multiplied. To take systematic uncertainties on the integrated luminosity, Q-square scales, and P_T boosting of the IVB + photon system into account, as well as uncertainties in our background estimate, we smeared the predicted number of events with the combined systematic uncertainty. (We added all uncertainties in quadrature in each bin, assuming gaussian errors. This is a good approximation of the more complicated reality, since the fluctuations are relatively small) Technically, this was done by generating 60 different CDF experiments, in each of which the nominal number of events is changed by a fraction. Each experiment gets weighted with the (truncated gaussian) probability density of having deviated from the mean $\mu_i(\Delta\kappa, \lambda)$ by the chosen amount. All of these probability densities are added and the logarithm of the sum taken.

$$\mathcal{P} = \prod_i^{nbins} \frac{e^{-\mu_i(\Delta\kappa,\lambda)} \cdot \mu_i(\Delta\kappa,\lambda)^{N_i}}{(N_i)!}$$

Adding in systematics we have:

$$\mathcal{L}(\cdot\kappa, \lambda) = \ln \int_0^{+\infty} \prod_i^{nbins} \left(\frac{e^{-\mu_i(\Delta\kappa,\lambda)+sys_i(x)} \cdot (\mu_i(\Delta\kappa,\lambda)+sys_i(x))^{N_i}}{(N_i)!}\right) \cdot GAU(x)dx$$

A similar technique is described in [11]. This log likelihood is a function of the anomalous couplings: in the case of $WW\gamma$ couplings, there are the two CP-conserving couplings $\Delta\kappa$ and

λ as well as the two CP-violating couplings $\tilde{\kappa}$ and $\tilde{\lambda}$. In the case of $Z\gamma$couplings, there are the four h_{i0} parameters. By varying these couplings we obtained log-likelihood functions which allowed us to extract confidence level limits. Ideally, we should find simultaneous limits for all four anomalous couplings. This would, however, go beyond the means of proper display. Here we follow the tradition of finding limits in two dimensions by assuming the other two couplings to be consistent with the Standard Model. In the case of $WW\gamma$ couplings, we either assumed the CP-violating couplings or the CP-conserving couplings to agree with the SM. Note that there exist stringent *indirect* limits on the CP-violating couplings $\tilde{\kappa}$ and $\tilde{\lambda}$ inferred from the experimental limit on the neutron electric dipole moment ($d_n = 0$ at tree level in the SM) which are roughly 1000 times better than we are able to obtain with our present integrated luminosity. Our results on these CP-violating couplings are the world's first *direct* limits.

To obtain the two-dimensional limits, we varied each of the two chosen couplings in small steps and calculated the log-likelihood that the expected event numbers would be identical to our observation. In the case of the $W\gamma$system, we scanned a 500×500 matrix of 250000 pairs of couplings. Since we could not run that many Monte Carlo programs, we parameterized for each P_T bin the expected number of MC events as a function of the two couplings. Since the invariant amplitudes describing anomalous couplings for the $WW\gamma$ and/or $ZZ\gamma$, $Z\gamma\gamma$ vertex are *linear* in the anomalous couplings, then the most general description of the cross section or number of predicted events is an elliptical paraboloid with six coefficients:

$$\mu_i(\Delta\kappa, \lambda) = A_i + B_i \cdot \Delta\kappa + C_i \cdot \lambda + D_i \cdot \Delta\kappa^2 + E_i \cdot \lambda^2 + F_i \cdot \Delta\kappa \cdot \lambda$$

where i stands for the i^{th} P_T bin. We then extracted the values of couplings which lead to the largest log-likelihood as our central results, which, to no surprise, agree well with the SM values in all cases , and obtained the 1 standard deviation contour from all pairs of coupling constants where the log-likelihood was 0.5 below the maximum value. Likewise, the 90% CL limit contour was extracted from all points with log-likelihood 2.3 below the maximum, and for the 95% CL the difference in log-likelihood was 3. These log-likelihoods are displayed versus $\Delta\kappa$ and λ in Figure 13. Similar plots are shown for CP-violating couplings in Figure 14. The limit values for the various confidence levels are shown in tables 23 - 24. The limit contours for CP-conserving and CP-violating $W\gamma$ couplings are displayed in Figure 15. Higher-order electromagnetic moments of the W boson, the magnetic dipole (μ_W) and electric quadrupole (Q^e_W) moments, are related to $\Delta\kappa$ and λ by

$$\mu_W = \frac{e}{2M_W}(2 + \Delta\kappa + \lambda)$$
$$Q^e_W = -\frac{e}{M^2_W}(1 + \Delta\kappa - \lambda)$$

Similarly the relationship between $\tilde{\kappa}$ and $\tilde{\lambda}$ and the CP-violating electric dipole (d^e_W) and magnetic quadrupole (Q^m_W) moments are given by

$$d_W^e = \frac{e}{2M_W}(\tilde{\kappa} + \tilde{\lambda})$$
$$Q_W^m = -\frac{e}{M_W^2}(\tilde{\kappa} - \tilde{\lambda})$$

For presentation we define the following dimensionless (scaled) quantities:

$$g_W - 2 = \frac{\mu_W}{\mu_W^0} - 2 = \Delta\kappa + \lambda$$
$$q_W^e - 1 = \frac{Q_W^e}{Q_W^{e0}} - 1 = \Delta\kappa - \lambda$$
$$d_W - 1 = \frac{d_W^e}{d_W^{e0}} - 1 = \tilde{\kappa} + \tilde{\lambda}$$
$$q_W^m - 1 = \frac{Q_W^m}{Q_W^{m0}} - 1 = \tilde{\kappa} - \tilde{\lambda}$$

The terms $\mu_W^0 = \frac{eh}{2M_W}$, $Q_W^{e0} = -(\frac{eh}{M_W c})^2$, $d_W^{e0} = \frac{ehc}{M_W}$, and $Q_W^{m0} = (\frac{h}{M_W c})^2$ are the classical moments of the W. The corresponding contours for the anomalous electric and magnetic moment fractions of the W can be found in Figure 16. The contours for the combined electron and muon channels were obtained by simply adding the likelihood values for both channels and then applying the criteria as written above. From the combined $e + \mu$ limits we obtain two interesting pieces of information: the W magnetic dipole moment and electric quadrupole moment are both non-vanishing and positive at more than the 95% CL; and for saturation of the unitarity bound we can exclude in the $WW\gamma$ system compositeness scales Λ_W below 1.55 TeV at the 95% CL for CP-conserving anomalous couplings. The limit on Λ_W is $\sim$ 2.0 TeV for CP-violating couplings, for saturation of the unitarity bound. The limit values for the various confidence levels are shown in tables 25 - 26.

The fitting technique described above was also applied to the electron and muon $Z\gamma$ samples. Results were obtained for h_{30},h_{40} (CP-conserving couplings) and h_{10},h_{20} (CP-violating couplings). The log-likelihood plots are shown in Figures 17 and 19 and the corresponding contours in Figures 18 and 20. The limit values for the various confidence levels are shown in tables 27 - 28. From the combined $e + \mu$ results, for saturation of the unitarity bound we can exclude in the $ZZ\gamma$ system compositeness scales Λ_Z below 500 GeV at 95% CL.

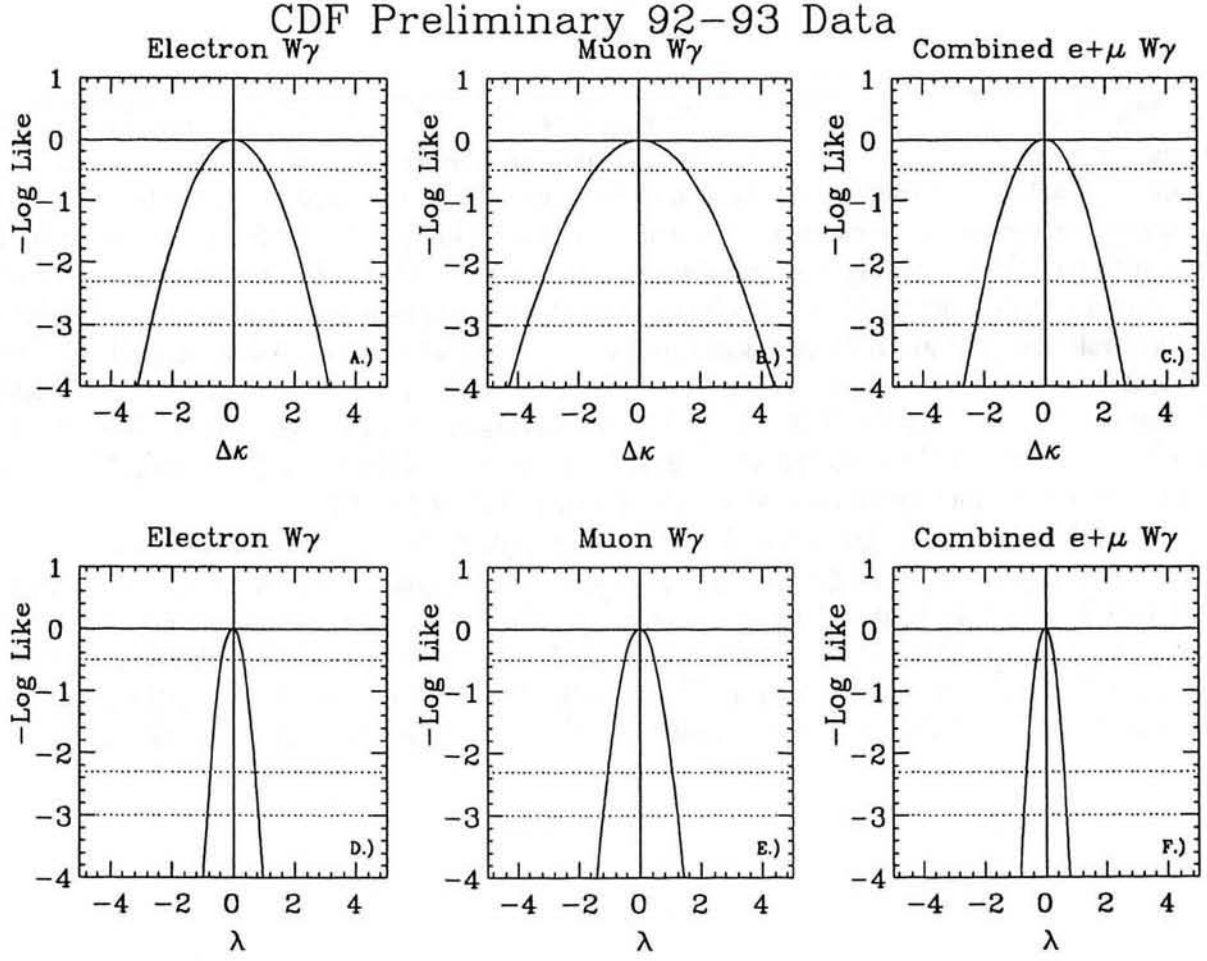
CDF Preliminary 92−93 Data
Electron Wγ
Muon Wγ
Combined e+μ Wγ
−Log Like
Δκ
λ
A.)
B.)
C.)
D.)
E.)
F.)

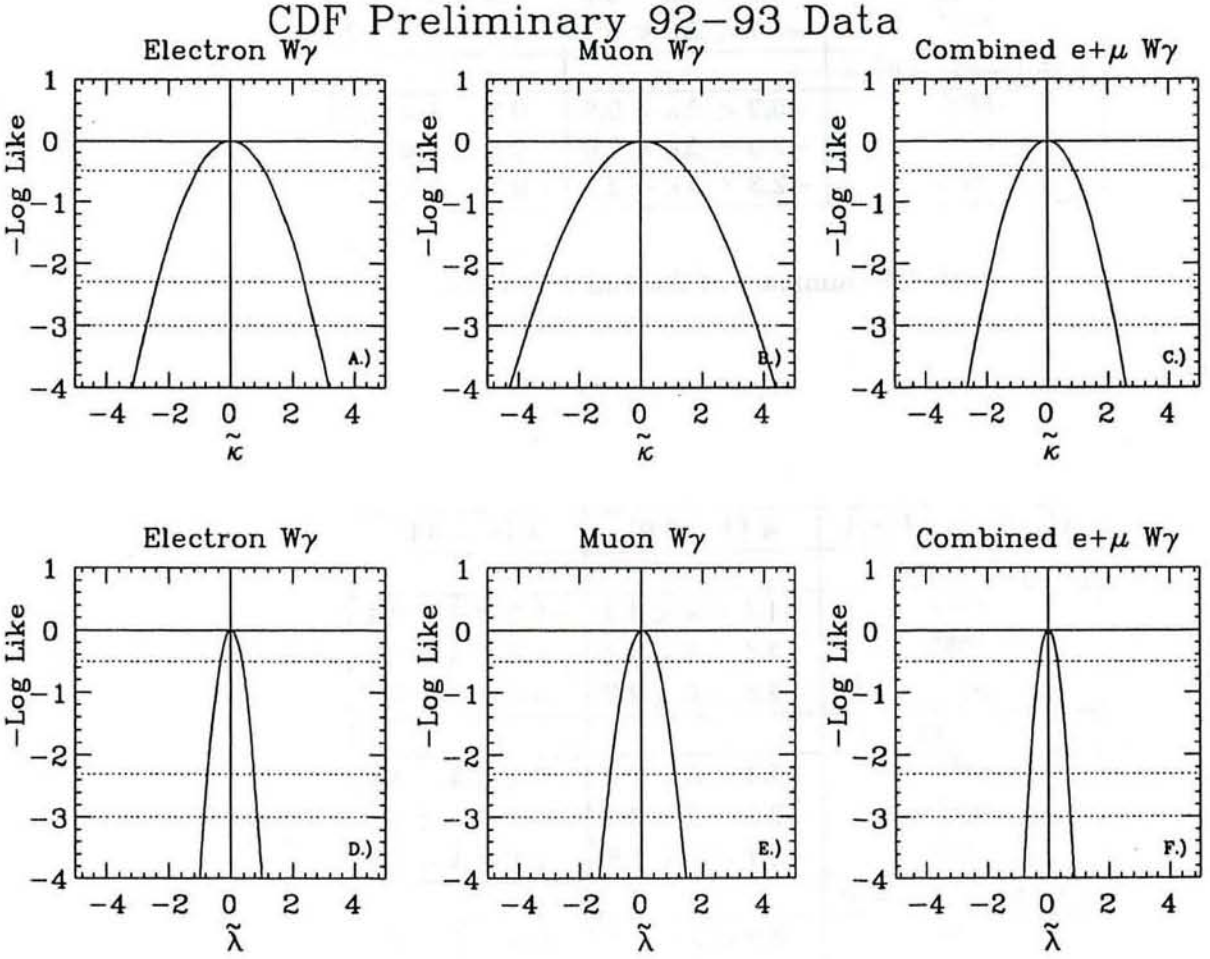
CDF Preliminary 92−93 Data
Electron Wγ
Muon Wγ
Combined e+μ Wγ
−Log Like
A.)
B.)
C.)
κ̃
Electron Wγ
Muon Wγ
Combined e+μ Wγ
−Log Like
D.)
E.)
F.)
λ̃

Confidence Level	$\Delta\kappa$ ($\lambda = 0.0$)	λ ($\Delta\kappa = 0.0$)
Electrons		
68%	$-1.2 < \Delta\kappa < 1.1$	$-0.4 < \lambda < 0.3$
90%	$-2.4 < \Delta\kappa < 2.4$	$-0.8 < \lambda < 0.8$
95%	$-2.8 < \Delta\kappa < 2.7$	$-0.9 < \lambda < 0.9$
Muons		
68%	$-1.5 < \Delta\kappa < 1.5$	$-0.5 < \lambda < 0.4$
90%	$-3.2 < \Delta\kappa < 3.2$	$-1.0 < \lambda < 1.0$
95%	$-3.7 < \Delta\kappa < 3.7$	$-1.2 < \lambda < 1.2$
Combined e and μ		
68%	$-0.9 < \Delta\kappa < 0.9$	$-0.3 < \lambda < 0.3$
90%	$-2.0 < \Delta\kappa < 2.0$	$-0.6 < \lambda < 0.6$
95%	$-2.3 < \Delta\kappa < 2.2$	$-0.7 < \lambda < 0.7$

Table 23: Summary of $\Delta\kappa$ and λ Results.

Confidence Level	$\tilde{\kappa}$ ($\tilde{\lambda} = 0.0$)	$\tilde{\lambda}$ ($\tilde{\kappa} = 0.0$)
Electrons		
68%	$-1.1 < \tilde{\kappa} < 1.1$	$-0.3 < \tilde{\lambda} < 0.4$
90%	$-2.4 < \tilde{\kappa} < 2.4$	$-0.7 < \tilde{\lambda} < 0.8$
95%	$-2.8 < \tilde{\kappa} < 2.7$	$-0.9 < \tilde{\lambda} < 0.9$
Muons		
68%	$-1.4 < \tilde{\kappa} < 1.5$	$-0.4 < \tilde{\lambda} < 0.5$
90%	$-3.2 < \tilde{\kappa} < 3.3$	$-1.0 < \tilde{\lambda} < 1.1$
95%	$-3.7 < \tilde{\kappa} < 3.8$	$-1.2 < \tilde{\lambda} < 1.2$
Combined e and μ		
68%	$-0.9 < \tilde{\kappa} < 0.9$	$-0.3 < \tilde{\lambda} < 0.3$
90%	$-2.0 < \tilde{\kappa} < 1.9$	$-0.6 < \tilde{\lambda} < 0.6$
95%	$-2.3 < \tilde{\kappa} < 2.2$	$-0.7 < \tilde{\lambda} < 0.7$

Table 24: Summary of $\tilde{\kappa}$ and $\tilde{\lambda}$ Results.

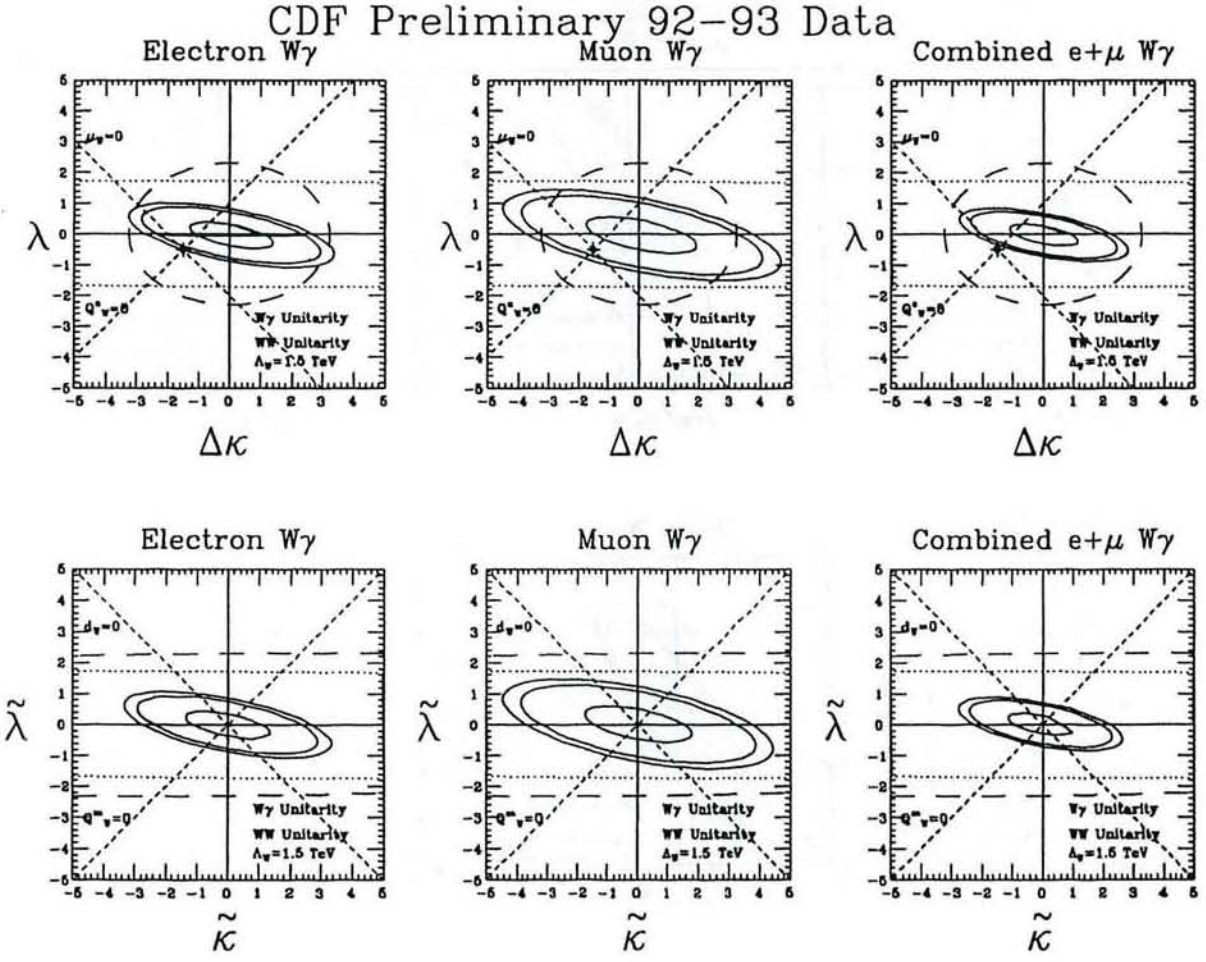
CDF Preliminary 92–93 Data
Electron Wγ
Muon Wγ
Combined e+μ Wγ
λ
Δκ
λ̃
κ̃
Wγ Unitarity
WW Unitarity
Λ=1.5 TeV

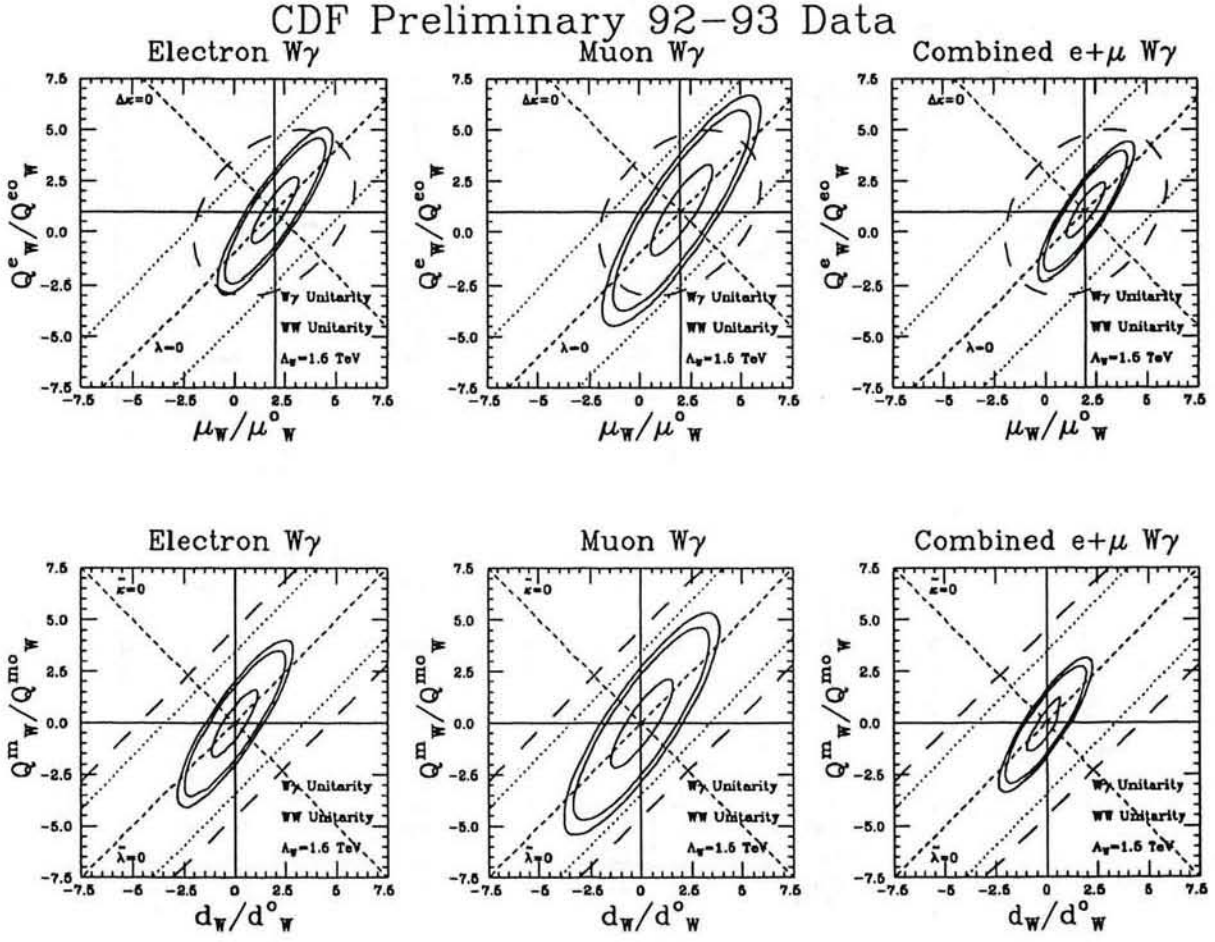
CDF Preliminary 92–93 Data
Electron Wγ
Muon Wγ
Combined e+μ Wγ
Q^e_W/Q^{eo}_W
μ_W/μ^o_W
Δκ=0
λ=0
Wγ Unitarity
WW Unitarity
Λ_w=1.5 TeV
Q^m_W/Q^{mo}_W
d_W/d^o_W

Confidence Level	g_W ($q_W^e = 1.0$)	q_W^e ($g_W = 2.0$)
Electrons		
68%	$-0.6 < g_W - 2 < 0.5$	$-0.8 < q_W^e - 1 < 0.9$
90%	$-1.3 < g_W - 2 < 1.2$	$-1.7 < q_W^e - 1 < 1.8$
95%	$-1.5 < g_W - 2 < 1.4$	$-1.9 < q_W^e - 1 < 2.0$
Muons		
68%	$-0.8 < g_W - 2 < 0.7$	$-1.1 < q_W^e - 1 < 1.2$
90%	$-1.7 < g_W - 2 < 1.6$	$-2.4 < q_W^e - 1 < 2.5$
95%	$-2.0 < g_W - 2 < 1.9$	$-2.7 < q_W^e - 1 < 2.8$
Combined e and μ		
68%	$-0.5 < g_W - 2 < 0.4$	$-0.6 < q_W^e - 1 < 0.7$
90%	$-1.1 < g_W - 2 < 1.0$	$-1.4 < q_W^e - 1 < 1.5$
95%	$-1.2 < g_W - 2 < 1.1$	$-1.6 < q_W^e - 1 < 1.7$

Table 25: Summary of Limits on W Boson CP-Conserving EM Moments.

Confidence Level	d_W ($q_W^m = 1.0$)	q_W^m ($d_W = 1.0$)
Electrons		
68%	$-0.6 < d_W - 1 < 0.5$	$-0.8 < q_W^m - 1 < 0.9$
90%	$-1.3 < d_W - 1 < 1.2$	$-1.6 < q_W^m - 1 < 1.8$
95%	$-1.5 < d_W - 1 < 1.4$	$-1.9 < q_W^m - 1 < 2.0$
Muons		
68%	$-0.8 < d_W - 1 < 0.8$	$-1.0 < q_W^m - 1 < 1.2$
90%	$-1.7 < d_W - 1 < 1.7$	$-2.4 < q_W^m - 1 < 2.5$
95%	$-2.0 < d_W - 1 < 2.0$	$-2.6 < q_W^m - 1 < 2.8$
Combined e and μ		
68%	$-0.5 < d_W - 1 < 0.4$	$-0.7 < q_W^m - 1 < 0.7$
90%	$-1.1 < d_W - 1 < 1.0$	$-1.4 < q_W^m - 1 < 1.5$
95%	$-1.2 < d_W - 1 < 1.1$	$-1.6 < q_W^m - 1 < 1.7$

Table 26: Summary of Limits on W Boson CP-Violating EM Moments.

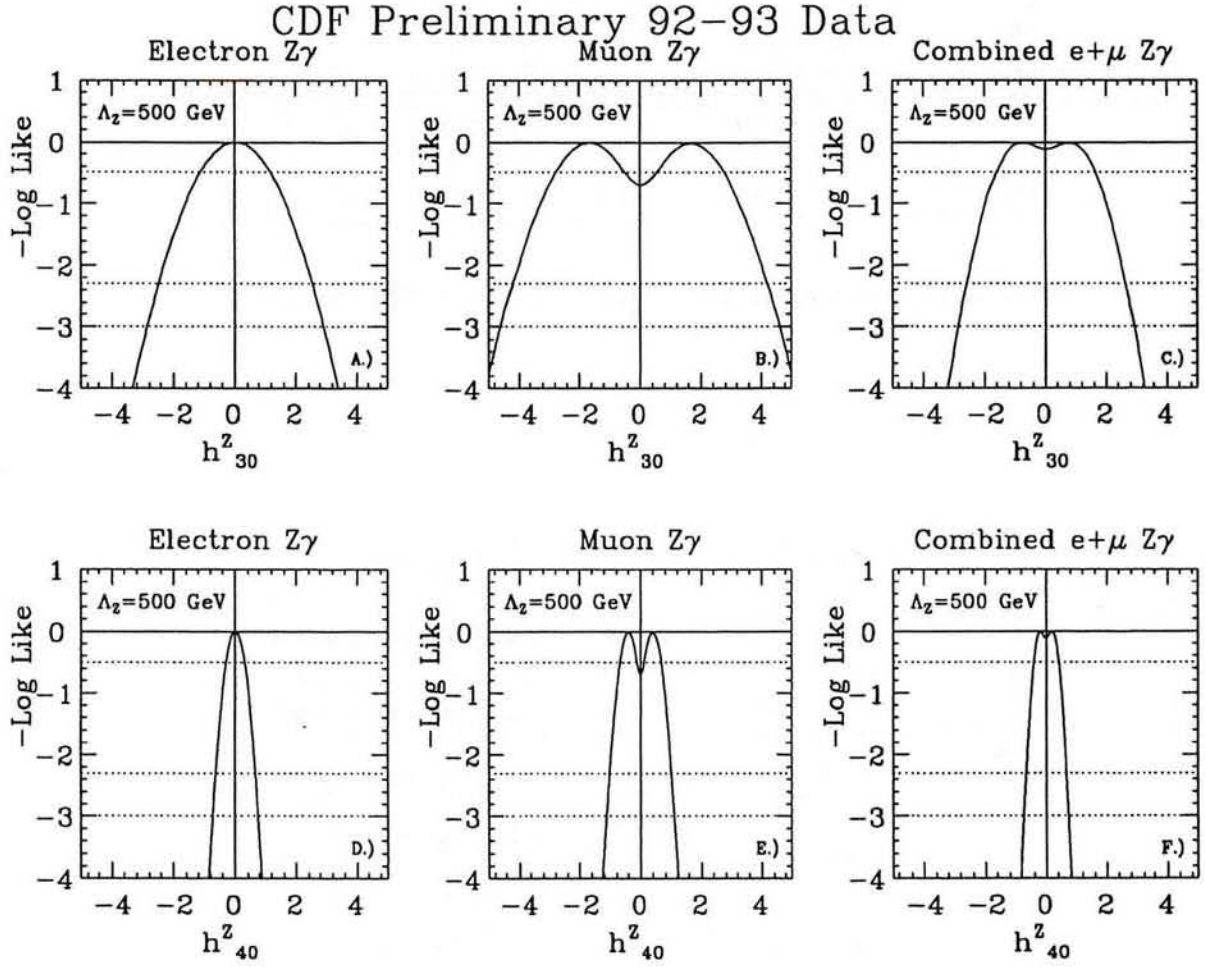
CDF Preliminary 92–93 Data
Electron Zγ
Muon Zγ
Combined e+μ Zγ
Λz=500 GeV
−Log Like
A.)
B.)
C.)
D.)
E.)
F.)
h^Z_30
h^Z_40

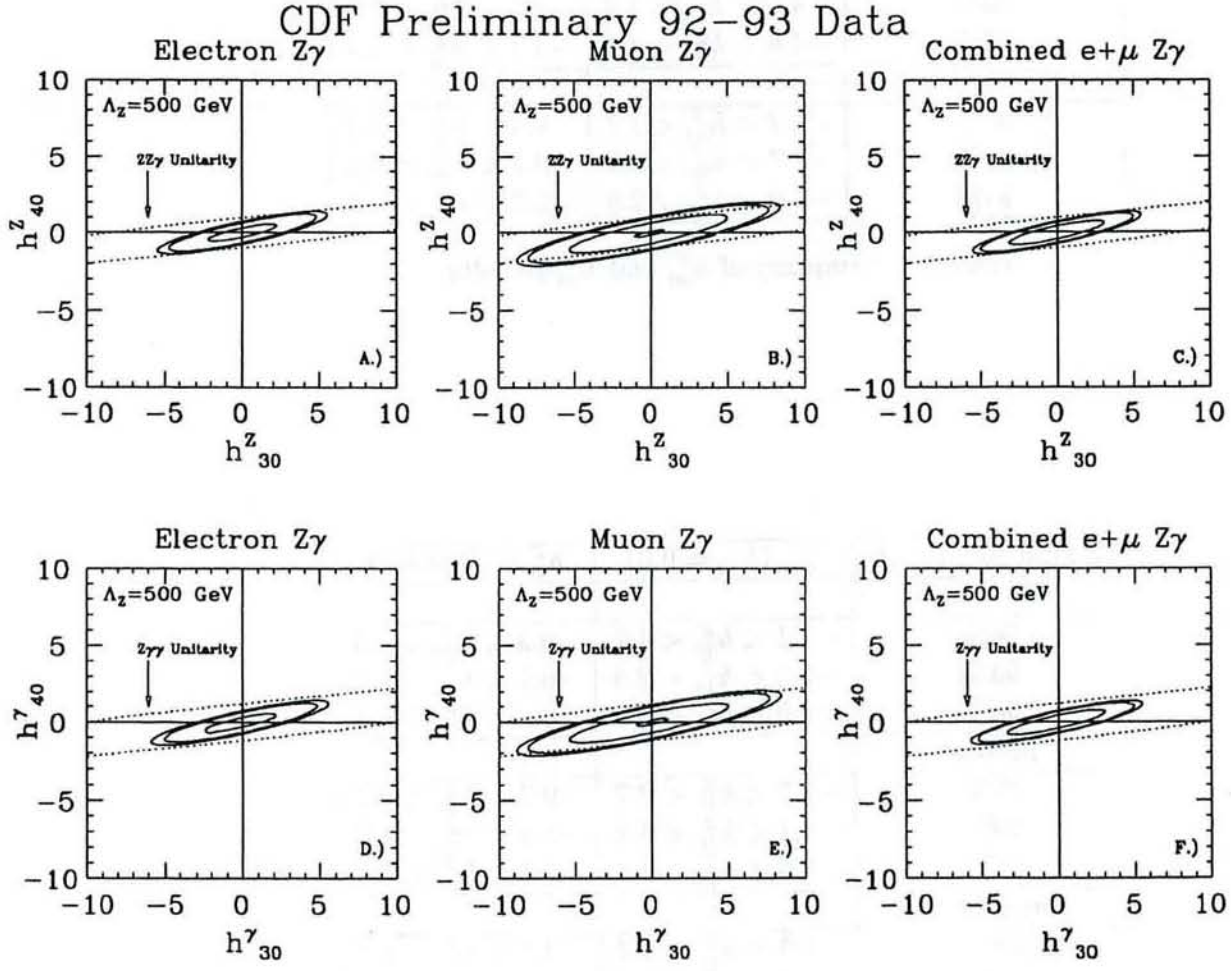
CDF Preliminary 92−93 Data
Electron Zγ
Muon Zγ
Combined e+μ Zγ
Λz=500 GeV
ZZγ Unitarity
Zγγ Unitarity
A.)
B.)
C.)
D.)
E.)
F.)
h^Z_40
h^Z_30
h^γ_40
h^γ_30

Confidence Level	h_{30}^Z ($h_{40}^Z = 0.0$)	h_{40}^Z ($h_{30}^Z = 0.0$)
Electrons		
68%	$-1.2 < h_{30}^Z < 1.2$	$-0.3 < h_{40}^Z < 0.3$
90%	$-2.6 < h_{30}^Z < 2.6$	$-0.6 < h_{40}^Z < 0.7$
95%	$-3.0 < h_{30}^Z < 2.9$	$-0.7 < h_{40}^Z < 0.8$
Muons		
68%	$-2.7 < h_{30}^Z < 2.8$	$-0.7 < h_{40}^Z < 0.7$
90%	$-4.2 < h_{30}^Z < 4.2$	$-1.0 < h_{40}^Z < 1.0$
95%	$-4.6 < h_{30}^Z < 4.6$	$-1.1 < h_{40}^Z < 1.1$
Combined e and μ		
68%	$-1.7 < h_{30}^Z < 1.7$	$-0.4 < h_{40}^Z < 0.4$
90%	$-2.7 < h_{30}^Z < 2.7$	$-0.7 < h_{40}^Z < 0.6$
95%	$-3.0 < h_{30}^Z < 2.9$	$-0.7 < h_{40}^Z < 0.7$

Table 27: Summary of h_{30}^Z and h_{40}^Z Results.

Confidence Level	h_{10}^Z ($h_{20}^Z = 0.0$)	h_{20}^Z ($h_{10}^Z = 0.0$)
Electrons		
68%	$-1.1 < h_{10}^Z < 1.2$	$-0.3 < h_{20}^Z < 0.3$
90%	$-2.5 < h_{10}^Z < 2.6$	$-0.7 < h_{20}^Z < 0.7$
95%	$-2.9 < h_{10}^Z < 3.0$	$-0.8 < h_{20}^Z < 0.8$
Muons		
68%	$-2.7 < h_{10}^Z < 2.7$	$-0.7 < h_{20}^Z < 0.7$
90%	$-4.1 < h_{10}^Z < 4.2$	$-1.0 < h_{20}^Z < 1.0$
95%	$-4.6 < h_{10}^Z < 4.6$	$-1.1 < h_{20}^Z < 1.1$
Combined e and μ		
68%	$-1.6 < h_{10}^Z < 1.7$	$-0.4 < h_{20}^Z < 0.4$
90%	$-2.6 < h_{10}^Z < 2.7$	$-0.7 < h_{20}^Z < 0.7$
95%	$-2.9 < h_{10}^Z < 3.0$	$-0.7 < h_{20}^Z < 0.7$

Table 28: Summary of h_{10}^Z and h_{20}^Z Results.

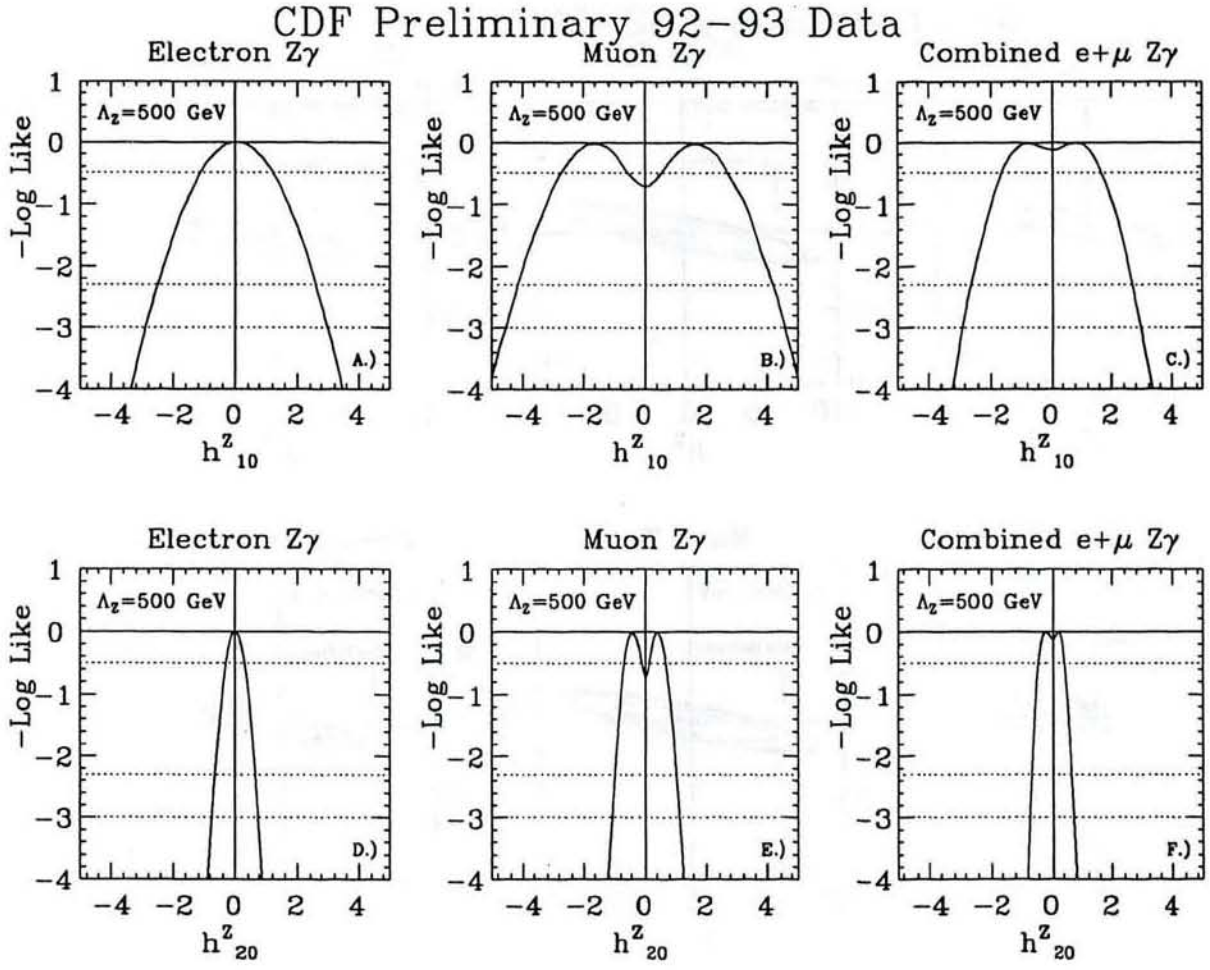
CDF Preliminary 92–93 Data
Electron Zγ
Muon Zγ
Combined e+μ Zγ
Λz=500 GeV
−Log Like
A.)
B.)
C.)
D.)
E.)
F.)
h^Z_10
h^Z_20

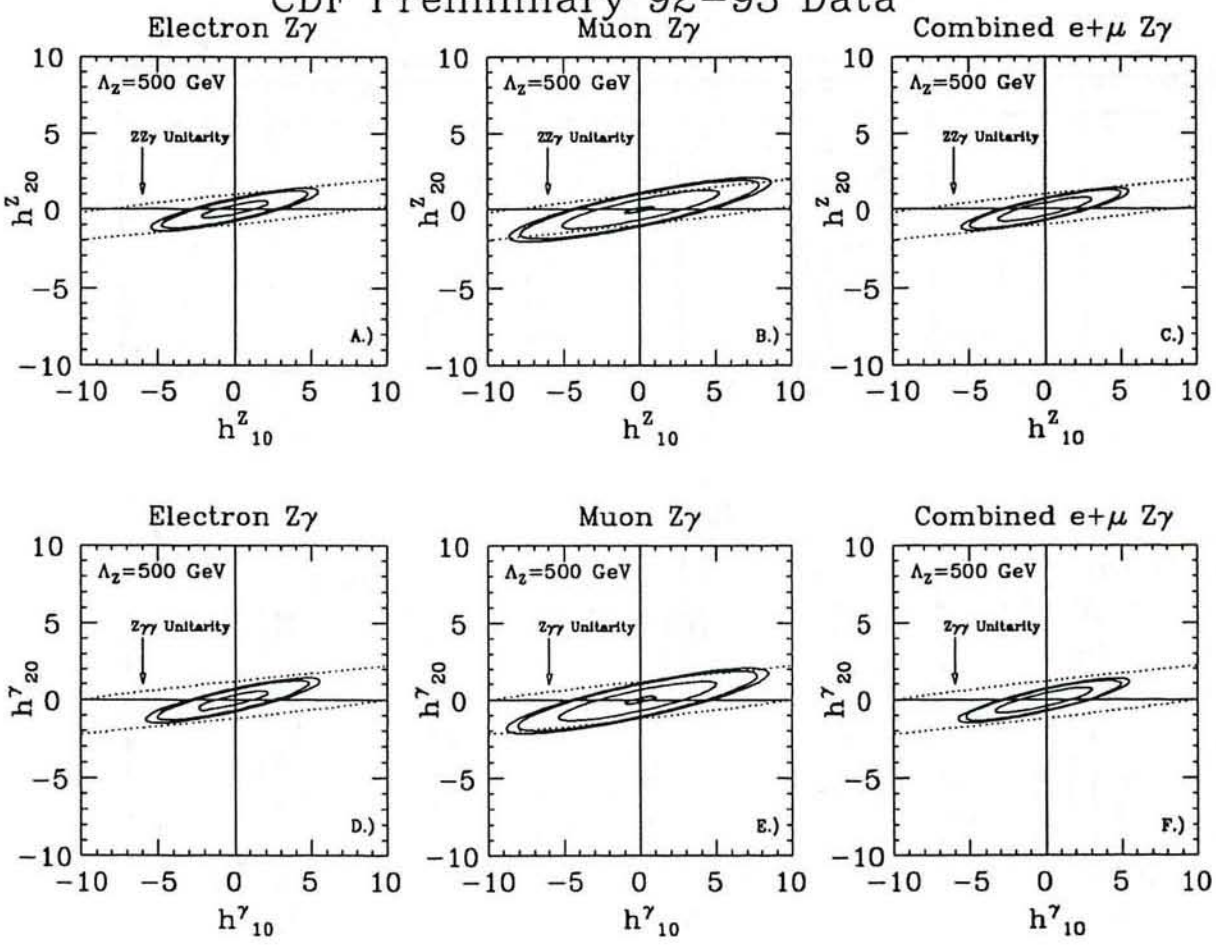
CDF Preliminary 92−93 Data
Electron Zγ
Muon Zγ
Combined e+μ Zγ
Λz=500 GeV
ZZγ Unitarity
Zγγ Unitarity
A.)
B.)
C.)
D.)
E.)
F.)
h^Z_20
h^Z_10
h^γ_20
h^γ_10

10 Summary

Using data from the 92/93 run we have determined the $W\gamma$ and $Z\gamma$ cross sections times branching ratio for central photons with a minimum transverse momentum of 7 GeV and a minimum separation from the decay lepton of $\Delta R = 0.7$. We found,

$$\sigma * BR(W\gamma)_e = 14.9^{+6.4}_{-6.4}\ (stat + syst)\ pb \qquad \sigma * BR(W\gamma)_\mu = 8.0^{+5.8}_{-5.8}\ (stat + syst)\ pb$$
$$\sigma * BR(W\gamma)_{SM} = 18.6^{+2.8}_{-2.8}\ (stat + syst)\ pb$$

$$\sigma * BR(Z\gamma)_e = 3.5^{+2.7}_{-2.7}\ (stat + syst)\ pb \qquad \sigma * BR(Z\gamma)_\mu = 6.3^{+4.2}_{-4.2}\ (stat + syst)\ pb$$
$$\sigma * BR(Z\gamma)_{SM} = 4.8\ ^{+0.6}_{+0.6}\ (stat)\ pb$$

We have determined limits on the CP-conserving anomalous couplings $\Delta\kappa$ and λ for each $W\gamma$ channel to be, at the 95% confidence level,

$$\begin{array}{lll} W\gamma_e & \rightarrow -2.8 < \Delta\kappa < 2.7 & -0.9 < \lambda < 0.9 \\ W\gamma_\mu & \rightarrow -3.7 < \Delta\kappa < 3.7 & -1.2 < \lambda < 1.2 \\ W\gamma_{e\mu} & \rightarrow -2.2 < \Delta\kappa < 2.2 & -0.8 < \lambda < 0.7 \end{array}$$

whereas both coupling values are predicted to be 0 for the Standard Model at tree level. From the limits on $\Delta\kappa$ and λ it is possible to extract limits on electromagnetic multipole moments of the W boson, specifically the electric quadrupole and magnetic dipole moments [1]. We find these limits to be, at the 95% confidence level,

$$\begin{array}{lll} W\gamma_e & \rightarrow -1.5 < g_W - 2 < 1.4 & -1.9 < q^e_W - 1 < 2.0 \\ W\gamma_\mu & \rightarrow -2.0 < g_W - 2 < 1.9 & -2.7 < q^e_W - 1 < 2.8 \\ W\gamma_{e\mu} & \rightarrow -1.2 < g_W - 2 < 1.2 & -1.6 < q^e_W - 1 < 1.7 \end{array}$$

We have also determined limits on the CP-violating anomalous couplings, $\tilde{\kappa}$ and $\tilde{\lambda}$, for each $W\gamma$ channel to be, at the 95% confidence level,

$$\begin{array}{lll} W\gamma_e & \rightarrow -2.8 < \tilde{\kappa} < 2.7 & -0.9 < \tilde{\lambda} < 0.9 \\ W\gamma_\mu & \rightarrow -3.7 < \tilde{\kappa} < 3.7 & -1.2 < \tilde{\lambda} < 1.2 \\ W\gamma_{e\mu} & \rightarrow -2.3 < \tilde{\kappa} < 2.2 & -0.7 < \tilde{\lambda} < 0.7 \end{array}$$

whereas both values are predicted to be 0 for the Standard Model at tree level. From the limits on $\tilde{\kappa}$ and $\tilde{\lambda}$ it is possible to extract limits on electromagnetic multipole moments of the W boson, specifically the electric dipole and magnetic quadrupole moments [1]. We find these limits to be, at the 95% confidence level,

$$\begin{array}{lll} W\gamma_e & \rightarrow -1.5 < d_W - 1 < 1.4 & -1.9 < q^m_W - 1 < 2.0 \\ W\gamma_\mu & \rightarrow -2.0 < d_W - 1 < 2.0 & -2.6 < q^m_W - 1 < 2.8 \\ W\gamma_{e\mu} & \rightarrow -1.2 < d_W - 1 < 1.1 & -1.6 < q^m_W - 1 < 1.7 \end{array}$$

Our results for $W\gamma$ processes are in good agreement with Standard Model predictions. We find that the W boson is a pointlike object up to compositeness scales of $\Lambda_W = 1.55$ TeV (95% CL), for saturation of the unitarity bound.

We have obtained limits on the CP-conserving anomalous couplings h_{30}^Z and h_{40}^Z for each $Z\gamma$ channel, for $\Lambda_Z = 500$ GeV. At the 95% confidence level, these are:

$$\begin{array}{lll} Z\gamma_e & \rightarrow -2.9 < h_{30}^Z < 3.0 & -0.8 < h_{40}^Z < 0.8 \\ Z\gamma_\mu & \rightarrow -4.6 < h_{30}^Z < 4.6 & -1.1 < h_{40}^Z < 1.1 \\ Z\gamma_{e\mu} & \rightarrow -2.9 < h_{30}^Z < 3.0 & -0.7 < h_{40}^Z < 0.7 \end{array}$$

whereas both coupling values are predicted to be 0 for the Standard Model at tree level. The limits on CP-violating anomalous couplings h_{10}^Z and h_{20}^Z for each $Z\gamma$ channel, for $\Lambda_Z = 500$ GeV, at the 95% confidence level are:

$$\begin{array}{lll} Z\gamma_e & \rightarrow -2.9 < h_{10}^Z < 3.0 & -0.8 < h_{20}^Z < 0.8 \\ Z\gamma_\mu & \rightarrow -4.6 < h_{10}^Z < 4.6 & -1.1 < h_{20}^Z < 1.1 \\ Z\gamma_{e\mu} & \rightarrow -2.9 < h_{10}^Z < 3.0 & -0.7 < h_{20}^Z < 0.7 \end{array}$$

The values of all four parameters are predicted to be 0 for the Standard Model at tree level.

Our results for $Z\gamma$ processes are also in good agreement with Standard Model predictions. We find that the Z boson is a pointlike object up to compositeness scales of $\Lambda_Z = 500$ GeV (95% CL), for saturation of the unitarity bound.

11 References

References

[1] D. Benjamin et al. **CDF-1941** (1993).

[2] S. Kopp, **CDF-2130** (1993).

[3] B. Badgett, **CDF-2217** (1993).

[4] S. Kopp, G. Sullivan **CDF-1942** (1993).

[5] Ulrich Baur, **CDF-1630**, includes modifications made by S. Errede.

[6] M. Lindgren, **CDF-1952** (1993).

[7] PDFLIB v4.15 by H. Plothow-Besch (1993).

[8] Mark Dickson, (1993).

[9] F. Abe *et al*, Phys. Rev. Lett. **67**, 2937 (1991).

[10] U. Baur *et al*, Phys. Rev. D **48**, (1993) 5140.

[11] F. James, Computer Physics Communication 20 (1980), R. J. Hollebeek et al., CDF-1109.